DEVOLATILIZATION CHARACTERISTICS OF CELLULOSE, HEMICELLULOSE, LIGNIN AND THE SELECTED BIOMASS DURING THERMOCHEMICAL GASIFICATION: EXPERIMENT AND MODELING STUDIES

By

VAMSEE PASANGULAPATI

Bachelor of Technology in Mechanical Engineering
Jawaharlal Nehru Technological University
Hyderabad, Andhra Pradesh, India
2007

Master of Science in Mechanical & Aerospace Engineering
Oklahoma State University
Stillwater, OK
2010

Submitted to the Faculty of the
Graduate College of the
Oklahoma State University
in partial fulfillment of
the requirements for
the Degree of
MASTERS OF SCIENCE
May, 2012

DEVOLATILIZATION CHARACTERISTICS OF CELLULOSE, HEMICELLULOSE, LIGNIN AND THE SELECTED BIOMASS DURING THERMOCHEMICAL GASIFICATION: EXPERIMENT AND MODELING STUDIES

Thesis Approved:

Dr. Ajay Kumar

Thesis Adviser

Dr. Carol L. Jones

Dr. Mark R. Wilkins

Dr. Sheryl A. Tucker

Dean of the Graduate College

.

TABLE OF CONTENTS

Chapter **Page**

Chapter **Page**

LIST OF TABLES

CHAPTER II

Table **Page**

CHAPTER III

CHAPTER IV

LIST OF FIGURES

CHAPTER II

Figure **Page**

Figure **Page**

CHAPTER III

CHAPTER IV

Figure **Page**

CHAPTER I

Introduction

Thermochemical conversion is one of the major pathways in converting biomass into liquid or gaseous fuels. In this process, heat is applied to break down biomass polymers into smaller molecules. Gasification and pyrolysis are two well-known thermochemical conversion technologies that are gaining worldwide attention. Gasification occurs in the presence of an oxidizing atmosphere and the final product is gaseous fuel known as syngas or producer gas. On the other hand, pyrolysis occurs in inert atmosphere and the final product is primarily a liquid fuel known as bio-oil. Even though the operation conditions such as temperature, heating rate and particle size required for these processes are different, the initial breaking down of biomass is similar. The process of breaking down biomass into volatiles with the application of heat in inert atmosphere is called as devolatilization or primary pyrolysis. This process is instantaneous and is the first phenomenon that occurs in any thermochemical conversion process following the drying of biomass. Thus, it is essential to study the fundamentals of biomass devolatilization, which helps in better understanding, modeling and optimization of biomass thermochemical conversion.

In chapter II, devolatilization characteristics of three major biomass components (cellulose, hemicellulose and lignin) were investigated using a thermogravimetric analysis technique. Spectral analysis was conducted using a Fourier Transform Infrared Spectrometer (FTIR) to investigate the evolution of gases such as CO, CO_2 and CH_4. The contribution of biomass components on thermal decomposition and gas releasing properties of biomass were investigated by comparing their devolatilization characteristics with those of switchgrass. In addition to major gases, hydrocarbons, aldehydes, and acids were also identified during thermal decompositions of switchgrass and model components.

In chapter III, the focus of the study was on comparing and contrasting biomass based on their compositions on evolution patterns of product gases and carbon conversion efficiency during thermochemical conversions. Switchgrass (SG), wheat straw (WS), eastern red cedar (ER) and dry distilled grains with solubles (DDGS) were used as biomass materials. These biomass materials were selected due to their significant variation in contents of cellulose, hemicellulose and lignin. Thermal decomposition characteristics of the selected biomass were investigated using a thermogravimetric analysis technique. FTIR was calibrated to quantify CO, CO_2 and CH_4; whereas, mass spectrometry (MS) was calibrated for argon gas.

In chapter IV, the focus of the study was to develop a computational fluid dynamics (CFD) model to simulate switchgrass gasification using kinetics developed for devolatilization. The kinetic parameters such as activation energy (E), pre exponential factor (A) and order of the reaction (n) developed for switchgrass decomposition were used to model devolatilization reactions.

Overall, this project focused on investigating devolatilization characteristics of biomass with varying contents of cellulose, hemicellulose and lignin to better understand, model and optimize biomass gasification process.

The specific objectives were to:

1. determine the weight loss kinetics of models of its biochemical components i.e. cellulose, xylan, lignin, separately during their devolatilization,
2. conduct spectral analysis to identify the volatiles including permanent gases, hydrocarbons, alcohols, acids and aldehydes evolved during devolatilization of model components,
3. compare and contrast biomass based on their compositions on evolution patterns of product gases and carbon conversion efficiency during thermochemical conversions,
4. develop a CFD based switchgrass gasification model using Arrhenius reaction rates and predict temperature and product concentration distributions inside a gasifier, and
5. examine the sensitivity and validation of the model by comparing the predicted outlet concentrations for different equivalence ratios with experimental data.

CHAPTER II

Characterization of switchgrass, cellulose, hemicellulose and lignin for thermochemical conversions

Abstract:

There is much interest in using switchgrass as a potential feedstock to produce energy and fuels**.** Thermochemical conversions, such as gasification and pyrolysis, are efficient ways of converting switchgrass into energy and fuels. The goal of this study was to investigate reaction kinetics and the nature of volatiles evolved during the thermochemical conversions of switchgrass and the contributions of its cellulose, hemicellulose and lignin to the decomposition. To accomplish this, a thermogravimetric analyzer (TGA) coupled with a Fourier Transform Infrared Spectrometer (FTIR) was used. Weight loss kinetics and a gas evolution profile of switchgrass and its components were analyzed under inert and oxidizing conditions. Significant weight loss of switchgrass occurred in the temperature range of 220 to 420 °C in nitrogen atmosphere and 220 to 390 °C in air atmosphere depending on heating rate.

The weight loss of the components occurred in different temperature ranges and also the reactivity of each component was different from one other. Among the components, cellulose decomposed sharply in a narrow temperature range with the highest mass loss; whereas, lignin decomposed in a wide temperature range with the lowest mass loss. The gases CO_2, CO and CH_4 were identified as major end products during switchgrass decomposition. As compared to lignin, cellulose and hemicellulose decomposition yielded higher CO and CO_2. However, most of the CH_4 yield was due to lignin decomposition.

Key words: Switchgrass, thermochemical conversion, weight loss kinetics, volatiles, cellulose, hemicellulose, lignin

1. Introduction

To meet the growing energy demands for transportation fuels and electrical power on a sustainable basis, it is necessary to find energy sources that are an alternative to fossil resources (Klass, 1995). Uses of fossil resources have also resulted in the release of underground trapped carbon into the atmosphere in the form of CO_2, a greenhouse gas. To help alleviate these concerns, use of biomass as an alternative energy sources has drawn growing interests worldwide. The efficient use of biomass for production of fuels and power can not only benefit the environment by recycling CO_2 but also provide opportunity to use biological waste materials such as agricultural, forestry and processing wastes (Biagini et al., 2006; Hall, 1997).

Among the available energy crops, switchgrass appears to be one of the most promising due to its higher biomass productivity, fast growth compared to other energy crops. In addition, low consumption of water, nutrients and pesticides makes production of switchgrass feasible (Keshwani & Cheng, 2009). Another significant advantage of switchgrass is its ability to use agricultural land without much degradation and carbon loss in soil (Massé et al., 2010).

Thermochemical conversion technologies such as pyrolysis and gasification are considered as efficient methods for converting biomass into fuels because these technologies can accept a wide variety of biomass feedstocks and generate a high fuel to feed ratio (Jeguirim & Trouvé, 2009; Kumar et al., 2008a). However, these processes involve enormous complex chain reactions and require knowledge of reaction kinetics (Lee & Fasina, 2009). An understanding of reaction kinetics during biomass

decomposition is essential in designing thermochemical units and modeling pyrolysis and gasification processes to predict product yields and properties (Miranda et al., 2007).

For understanding thermochemical processes, there is a need for an accurate technique that can simulate conditions similar to thermochemical conversions and predict the thermal degradation behavior of biomass effectively. Thermogravimetric Analysis (TGA) is one of the most commonly used techniques to understand the weight loss kinetics involved during biomass decomposition (Mani et al., 2010a). This analysis has been used to determine devolatilization kinetics of a variety of woods to distinguish the wood species based on their composition (Branca et al., 2005; Mészáros et al., 2004). TGA coupled with Fourier Transform Infrared Spectrometer (FTIR) provides even better understanding of fundamentals by characterizing the volatiles evolved during biomass degradation than TGA alone (Lee & Fasina, 2009). The TGA-FTIR technique has been used to understand the pyrolysis characteristics of variety of feedstocks. TG-FTIR technique was used in tobacco pyrolysis to analyze evolution patterns of pyrolysis products (Wang et al., 2011). The evolution patterns of pollutant gases from the pyrolysis of coal and biomass blends were examined by the same authors using TG-FITR. Guintoli et al. (2009) also used TGA-FTIR for product analysis from pyrolysis of agricultural waste. The pyrolysis of maize stalks, rice straw and cotton straw was carried out using TGA-FTIR and CO, CO_2, CH_4 were identified as major gaseous products (Fu et al., 2010). The effects of oxygen concentration and particle size on thermal degradation of olive solid waste were also investigated (Chouchene et al., 2010). The authors concluded that the temperature ranges of devolatilization and char oxidation were dependent on the size of olive solid waste. The effect of heating rate on the pyrolysis characteristics of

different biomass was investigated by various researchers (Haykiri-Acma et al., 2006; Mani et al., 2010b). Al-Harahsheh et al. (2011) observed that there was an increase in both activation energy and pre exponential factor with increasing the heating rate. Wang et al. (2009) pointed out that there was increase in the pyrolysis and oxidation rates of dry distilled grains with solubles with increase in the heating rate. Many studies on biomass components have been conducted to predict thermal behavior during biomass pyrolysis (Orfão et al., 1999; Yan et al., 2005). However, studies on identification of all volatiles during devolatilization of cellulose, hemicellulose and lignin and comparison with volatiles profile from biomass are scarce. The novelty of this study was the investigation of how biochemical components of switchgrass contributed to its weight loss and gas evolution profile during thermal decomposition. The specific objectives were to a) determine the weight loss kinetics of switchgrass, and models of its biochemical components i.e. Avicel cellulose as a model of cellulose, and xylan as a model of hemicellulose, and alkali lignin as a model of lignin, separately, under nitrogen and air atmospheres, and b) conduct spectral analysis to identify the volatiles including gases, hydrocarbons, alcohols, acids and aldehydes evolved during devolatilization of switchgrass and its model components.

2. Materials and Methods

2.1 Materials

Kanlow variety switchgrass (*Panicum virgatum*) grown at the Oklahoma State University Agronomy Research Station was used as the biomass feedstock . For thermogravimetric analysis, it was milled to 2 mm size using Thomas-Willey mill (Arthur H. Thomas Co., Philadelphia). The ultimate and proximate analyses of

switchgrass are presented in Table 1. The proximate analysis was performed following ASTM D-3172 and ASAE Standard S358.2. The ultimate analysis was performed by Midwest Microlab, LLC (Indianapolis, IN). Avicel PH 105 cellulose, xylan (processed from beachwood) and alkali lignin were used as three main models of cellulose, hemicellulose and lignin, respectively. Average particle size of Avicel PH 105 cellulose (FMC Corp, Newark, DE, USA) was 50 µm. Xylan (Sigma Aldrich, St. Louis) and alkali lignin (Sigma Aldrich, St. Louis) were purchased from Sigma-Aldrich Company. Although xylan might not represent hemicellulose completely, it is a major component of biomass hemicellulose and has been used as a model for hemicellulose in many studies (Biagini et al., 2006; Biagini & Tognotti; Vamvuka et al., 2003b). The average particle size of xylan and lignin were about 250 µm and 200 µm, respectively. All materials were dried at 104 °C for 24 hours prior to the thermogravimetric analysis.

2.2 Determination of chemical composition

For compositional analysis, switchgrass sample was sieved through +60/+400 (250 µm/38 µm sieve openings) sieve plates on a horizontal sieve shaker according to National Renewable Energy Laboratory (NREL) procedures (A. Sluiter, 2008a; Carrier et al., 2011). About 200 g of the sample was loaded into the sieve. More than 95% of the switchgrass was retained on +60 sieve plate. Switchgrass retained on this plate was used for extraction and compositional analysis. Water and ethanol extraction of biomass was carried using an accelerated solvent extractor (ASE) (Model 300, Dionex Corporation, Sunnyvale, CA) to remove the non-structural material using NREL protocols (A. Sluiter, 2008a). The weight of extractives was recorded after air drying.

Following extraction, the residual material was analyzed for structural carbohydrates, lignin, acetyl content and ash content using the two step acid hydrolysis procedure developed by NREL (A. Sluiter, 2008b; Mani et al., 2010b). For ash analysis and determination of acid insoluble lignin (AIL), a muffle furnace (Fisher Scientific, Dubuque, IA) was used. Structural carbohydrates were analyzed using a HPLC (Model 1100, Agilent Technologies, Santa Clara, CA) connected to a refractive index detector (RID) with an Bio-Rad Aminex HPX-87P column (Bio-Rad, Sunnyvale, CA). Deionized water was used as an eluent at a flow rate of 0.6 ml/min. The column was maintained at 85 °C. The total run time using this column was 30 min. The HPLC with Chemstation software (Agilent Technologies) was calibrated at five levels using known concentrations of compounds before being used to quantify the concentration of compounds. Acid soluble lignin (ASL) content of biomass was determined using a UV-Vis spectrophotometer (Cary 50 Bio, Varian Inc., Palo Alto, CA, USA) at a wavelength of 205 nm and an extinction coefficient of 110 L/g-cm.. The chemical composition of switchgrass were comparable to those reported by Wiselogel and Agblevor (1996) and Liu and Ye (2010) (Table 2).

2.3 Experimental methods

TGA (model: Versa Therm, ThermoFischer Scientific, USA) coupled with FTIR (model: Nicolet 6700, ThermoFischer Scientific, USA) was used for this this study. Switchgrass samples were heated from room temperature (25-30 °C) to 1000 °C at heating rates of 10 °C min^{-1}, 20 °C min^{-1} and 50 °C min^{-1}. Approximately 20 mg of sample was used for all the experiments to diminish the heat and mass transfer limitations within the sample (Shen et al., 2010). Purified nitrogen and air were used as purging

gases during all the experiments. A constant flow rate of 60 ml/min was maintained using an integrated mass flow controller to avoid longer residence times in TGA and thus to minimize secondary volatile interactions (Biagini et al., 2006). The evolved volatiles were immediately directed to the FTIR gas cell through a transfer line. The transfer line was heated to 225 °C to avoid condensation of volatiles. The mid infrared radiation absorbed by the sample was detected using a deuterated triglycine sulfate (DTGS) detector (Thermo Fischer Scientific, USA). The detector measured the absorption of the infrared light at different wavelengths based on the function groups presented in the volatile mixture. The infrared spectrum scanning ranged from 4000 to 400 cm^{-1} and each spectrum was obtained averaging 16 scans at a resolution of 1 cm^{-1}. FTIR absorbance spectra was obtained every 30s. Each volatile component was identified by matching the spectra with reference spectra available in the library database. Since several compounds evolved at the same time, subtraction method was used to identify the unknown components presented in the spectrum. This subtraction method isolated spectrum of know components from the spectrum of a gas mixture analyzed. The evolution patterns of major gases such as CO_2, CO and CH_4 were obtained by selecting absorbance band regions of 2250-2500 cm^{-1}, 2100-2250 cm^{-1} and 2850-3000 cm^{-1} respectively. All TG-FTIR experiments were repeated at least three times.

2.4 Determination of parameters of reaction kinetics

In the literature, numerous approaches were reported to determine the kinetic parameters such as activation energy, pre-exponential factor and order of the reaction during biomass decomposition. Since thermochemical processes involve many complex reactions, no single model can adequately represent the reaction kinetics of a variety of

biomasses (Biagini et al., 2009). The kinetic model used in this study is more generic and based on the Arrhenius equation. This model was successfully used by Kumar et al. (2008a) for corn stover, Chouchene et al. (2010) for olive waste and Mansaray and Ghaly (1999) for rice husk. The reaction kinetic parameters were determined using the following rate equation.

$$-\frac{dw}{dt} = kX^n \quad (1)$$

The reaction constant based on Arrhenius equation can be written as,

$$k = Ae^{-E/RT} \quad (2)$$

where, n is the order of the reaction, X is the weight of the sample (mg), A is the pre exponential factor , E is the activation energy (kJ mol^{-1}), T is the temperature (K) and R is the universal gas constant (kJ mol^{-1} K^{-1}).

The linearized form of Arrhenius equation was used to determine the reaction kinetic parameters by applying multi-linear regression technique. The simplified rate equation is shown below.

$$y = a + bX + cZ \quad (3)$$

Where,

$$y = ln\left[\frac{1}{w_f - w_i}\frac{dw}{dt}\right], x = \frac{1}{T}, z = ln\left(\frac{w - w_f}{w_i - w_f}\right),$$

$$a = ln(A), b = \left(\frac{-E}{R}\right), c = n$$

w is the weight of the sample at time t (mg),

w_i is the initial weight of the sample of the stage (mg),

w_f is the weight of the residue of that stage (mg)

The rate equation was integrated using the estimated constants (a, b and c), and the weight loss with respect to temperature was predicted. Microsoft excel (2007) software was used for multi linear regression. The simulated data was then compared with the experimental data.

3. Results and discussion

3.1 Under nitrogen conditions

3.1.1 Thermogravimetric analysis and reaction kinetics of cellulose, xylan and lignin

The weight loss and rate of weight loss profiles of cellulose, xylan and lignin are shown in Fig. 1 and Fig. 2. The weight loss of these components occurred in different temperature ranges and also the reactivity of each component was different from other. Xylan (representing hemicellulose) decomposed early in the temperature range of 200-315 °C with the maximum weight loss occurring in the range of 286-295 °C. The derivative plot of xylan showed two different peaks during its decomposition. The first peak could be due to the decomposition of side chains and the separation of glycosidic bonds from the xylan structure (Shafizadeh et al., 1972; Shen et al., 2010). The second peak can be attributed to the fragmentation of the main structure of xylan. The amount of solid residue remaining after complete decomposition was about 20 wt %. Cellulose pyrolyzed in a temperature range (290-400 °C) and the maximum mass loss was observed

at 349-355 °C. The final residue after the cellulose decomposition was about 4 wt. %. In contrast to the weight loss of cellulose and xylan, lignin decomposed slowly in a wider temperature range (200-900°C) and the final residue after its decomposition was ~51 wt.%.

The parameters of the reaction kinetics of cellulose, xylan and lignin are shown in Table 3. The differences in activation energies of these components might be attributed to the nature of their reactivity and structural differences. The activation energy (43 KJ.mol^{-1}) of lignin was very low compared with those of cellulose and xylan in the temperature range of 220-400 °C. Similar observations were made by Yang et al. (2004) and Vamuka et al (2003a). However, secondary weight loss of lignin was observed at higher temperature of 680-740 °C with activation energy of approximately 98 KJ.mol^{-1}. The weight loss in the higher temperature range might be due to the catalytic effect of alkali (Na_2CO_3) and ash content of lignin (Kumar, 2009). Among these three components, the activation energy of cellulose was highest (119 KJ.mol^{-1}). In the case of xylan, two distinct weight loss rate curves were observed within the temperature range of 200-315 °C as shown in Fig.1. The first curve was observed in the range of 200-260 °C with the activation energy of 116 kJ mol^{-1}. Similar observations for cellulose and hemicellulose were reported by Jeguirim and Trouve (2009) for different heating rates. In this study, a lower value of activation energy (58 kJ mol^{-1}) was obtained for xylan in the temperature range of 260-315 °C. Higher activation energy may be required in lower temperature range to separate the glycosidic bonds and side chains from xylan structure.

3.1.2 Thermogravimetric analysis and reaction kinetics of switchgrass

The weight loss and rate of weight loss profiles of switchgrass at different heating rates are shown in Fig. 3 and 4 respectively. With increase in heating rate, the peak for maximum rate of weight loss shifted towards higher temperatures. This might be attributed to the temperature gradients within the sample at high heating rates (Yang et al., 2004). Also, there was a minor increase in the end residue content with increase in the heating rate. At low heating rates, the heating of the switchgrass particles occurred slowly resulting in effective heat transfer within the particles. Hence, at lower heating rates, the cracking took place more effectively and resulted in more weight loss in the form of volatiles. The effect of heating rate on the weight loss profiles would be more prominent at heating rates higher than those used in this study. The switchgrass decomposition can be clearly divided into three stages. The first stage corresponding to moisture evaporation, ranged from 25 °C to about 125 °C. The second stage characterizing the weight loss of hemicellulose and cellulose ranged from 220 °C to about 400 °C depending on heating rate. During this stage of decomposition, about 70 wt % of switchgrass was lost. The final stage decomposition was primarily associated with the weight loss of lignin, ranging from 400 to 900 °C.

The temperature range of 220-400 °C was considered to determine the parameters of reaction kinetics of switchgrass devolatilization due to the major weight loss in this stage. The activation energy (E) and order of reaction (n) during switchgrass decomposition were calculated as 103.7 kJ mol^{-1} and 0.67, respectively (Table 3). These values are in close agreement with data provided by Munir et al.(2009) and Zhang et al.(2006), even though they used different feedstocks. The activation energy, pre exponential factor (A) and order of the reaction were used as inputs to predict the weight

loss profile of switchgrass. The simulated data well represented the actual weight loss profile (Fig. 5).

3.2. Under air conditions

3.2.1 Thermogravimetric analysis and reaction kinetics of cellulose, xylan and lignin

Fig. 6 and 7 show the decomposition of cellulose, xylan and lignin in oxidizing atmosphere. Each component decomposed with different reactivity and the temperature zone of decomposition varied from component to component. The major weight loss stage of xylan ranged from 180-285 °C and its decomposition continued until 900 °C. Cellulose started to decompose at about 235°C with about 86 % of its weight lost when it reached 355 °C. The slow degradation of lignin occurred in the temperature range of 210-835 °C and only about 38% of its weight was lost. Interestingly, about 43% of the lignin that was decomposed did so in the temperature range of 835-912 °C. The presence of alkali in the lignin may have promoted the weight loss in high temperature zone (Kumar, 2009). Reaction kinetic parameters were obtained for cellulose, xylan and lignin in air atmosphere (Table 4). The activation energy of cellulose (135 kJ mol^{-1}) in air atmosphere was higher than those in nitrogen atmosphere. However, xylan had only one peak with activation energy of 118 kJ mol^{-1}. Lignin had the lowest activation energy of 67 kJ mol^{-1} in the temperature range of 200-340 °C and highest activation energy of 160 kJ mol^{-1} in the range of 840-915 °C.

3.2.2 Thermogravimetric study and reaction kinetics of switchgrass

The effect of oxidizing atmosphere on switchgrass decomposition can be seen in Fig. 8. The weight loss behavior of switchgrass can be clearly separated into 3 stages.

The first stage of decomposition was attributed to moisture evaporation (25-125 °C). This stage of decomposition was similar to that of the first stage in nitrogen atmosphere. However, the second stage of decomposition was much sharper (220 to about 350-390 °C) under oxidizing conditions and it can be clearly evidenced from DTG curves (Fig. 9. The maximum rate of weight loss was much higher in oxidizing conditions than in an inert atmosphere. Moreover, the rate of weight loss reached its maximum value at a lower temperature than in nitrogen indicating the higher reactivity in air atmosphere. This might be attributed to the oxidation of hemicellulose and cellulose present in switchgrass. The final stage of weight loss ranged from 390-515°C for higher heating rates and 350-600°C for lower heating rates. Lignin was the main component that decomposed in this stage. The devolatilization of hemicellulose and cellulose followed by their ignition may have increased the porosity of the char formed in the second stage. Thus, oxygen may have diffused into this char and increased reactivity of lignin during the final stage of decomposition (Chouchene et al., 2010; Munir et al., 2009). The reaction kinetic parameters were obtained for switchgrass under oxidizing conditions. The activation energy (122 kJ mol^{-1}) and pre exponential factor (3.88×10^{10} s^{-1}) obtained in air atmosphere were higher than those in nitrogen atmosphere. This might be due to the rapid reactions occurring in the presence of oxygen in air atmosphere. The order of the reaction was less than one as shown in Table 4.

3.3 FTIR results

The volatiles released during decomposition of switchgrass and its components were identified using FTIR. Fig. 10 represents the stack plot of volatiles evolved during switchgrass decomposition. The plot was developed by superimposing the spectra

obtained every 5 s from 25-1000 °C. However, the characterization of all organic compounds evolved in the narrow temperature range was difficult to achieve because of limitation of FTIR. The major gases, such as CO_2, CO, CH_4, along with water were easily identified based on the specific wave number ranges. The integrated absorbance can be defined as integration of absorbance over a wave number range (specific to each compound) and it is proportional to the concentration of the chemical species presented in the evolved gases (Biagini et al., 2006). Two different wave number ranges of 2217-2391 cm^{-1} and 586-726 cm^{-1} indicated the formation of CO_2. The absorption bands in the wave number range of 586-726 cm-1 was due to the bending of O-C-O bonds. This wave number range was not considered for CO2 identification as the formation of other volatiles exists within same wave number range. The range of 2000-2250 cm^{-1} indicated the formation of CO. The absorption bands at wave number ranges of 2850-3000 cm^{-1} and 1470-1450 cm^{-1} evidenced the formation of CH4. The strong bands in the region of 2850-3000 cm-1 were due to C-H stretch and the weak bands in the region of 1470-1450 cm-1 were due to C-H bending. Thus, it was used to compare the behavior of volatile species evolved by switchgrass and its components under the similar operating conditions.

3.3.1 Chemical structure of switchgrass

The chemical structure of switchgrass was analyzed using FTIR. Fig. 11 shows the different chemical bands representing the typical structure of switchgrass. The band intensity at 3410 cm^{-1} indicated the presence of O-H groups in switchgrass. The absorption bands at 2937 cm^{-1} can be attributed to the C-H vibrations of aliphatic carbon. The presence of carbonyl groups in switchgrass was confirmed based on the peak at 1720

cm^{-1}. The bands in the range of 1700-1400 cm^{-1} indicated the existence of olefinic (C=C) functional groups. The strong intensities at 1040 cm^{-1} and 1220 cm^{-1} pointed out the asymmetric stretch of ether functional groups (C-O-C). The chemical bands in the fingerprint region (1000-650 cm^{-1}) were attributed to the bending vibrations of C-H groups.

3.3.2 Identification of volatiles during switchgrass pyrolysis

The thermal behavior of switchgrass was further investigated by understanding the evolution profiles of volatiles using FTIR technique. Three temperatures (115, 367 and 592 °C) corresponding to water evaporation, main stage of decomposition and final state of decomposition, respectively, were chosen to describe the pyrolysis of switchgrass. The absorption bands at 4000-3500 cm^{-1} and 1850-1250 cm^{-1} confirmed the evaporation of water in the initial stages of decomposition (Fig. 12).

As the pyrolysis process developed, the major products such as CO_2, CO andCH_4, along with some organic compounds evolved (Fig. 13). The switchgrass weight loss profile also confirmed this evolution of volatile products in this stage (Fig. 3). The characteristic bands at 2400-2240 cm^{-1} and 2240-2050 cm^{-1} indicated the formation of CO_2 and CO .The appearance of absorption bands of water in this stage could be due to the cracking of hydroxyl groups. Moreover, the bands developed at 3100-2750 cm^{-1} indicated the evolution of hydrocarbons such as CH_4, and C_2H_6. The presence of carbonyl (1765-1715 cm^{-1}), hydroxyl (3400-3200 cm^{-1}) andC-O-C (1250-1082 cm^{-1}) groups confirmed the evolution of acids, aldehydes, ketones, phenols and alcohols . Similar observations were reported by Yang et al. (2007). The wave numbers associated with particular functional groups are shown in Table 5.

Fig. 14 shows the IR profile of volatiles evolved during the final stage of decomposition at 590 °C. The absorption bands representing the carbonyl and hydroxyl groups were absent, and only the major gases, such as CO_2, CO with trace amounts of CH_4, were released in this stage. Gases with diatomic molecules such as H_2, N_2, and O_2 had no IR absorption; therefore, they were not detected by FTIR. In addition, no components containing nitrogen or sulfur were detected due to the low amounts of these elements present in switchgrass (Table 1).

3.3.3 The evolution characteristics of major gas products during pyrolysis

The evolution characteristics of CO_2, CO and CH_4 during decomposition of switchgrass were observed. All three components contributed to the formation of CO_2 (Fig 15). The cracking and reforming of carbonyl and carboxyl bonds may have resulted in the production of CO_2 (Fu et al., 2010). Release of CO_2 may have been mostly contributed by xylan at low temperatures (below 500 °C) (shown in Fig. 15). Similar observations were reported by Yang et al. (2007) and Fu et al. (2009). In the low temperature region, CO_2 contributions by cellulose and lignin could be much less than that of xylan. Previous studies indicated that cellulose pyrolysis contributed to only small amount of CO_2 (Li et al., 2001; Shen & Gu, 2009). As the temperature increased, cellulose may have released higher amounts of CO_2 and reached maximum at 576 °C. Lignin produced higher CO_2 in the temperature range of 800-900 °C which could be due to breaking of C-C, C-O and ether linkages between aromatics from the lignin structure.

The release profile of CO from switchgrass and its components is shown in Fig. 16. Xylan contributed to the higher amount of CO in the low temperature range (below

400 °C). The formation of CO at low temperatures may be because of cracking and reforming of ether (C-O-C) and carbonyl groups (C=O). Cellulose produced higher CO in high temperature range (above 400 °C). The secondary reactions of primary volatiles and aldehyde groups (R-CHO) probably resulted in higher CO. Almost negligible amount of CO was produced during lignin decomposition below 800 °C. The sharp increase in CO release above 800 °C could be due to the thermal cracking of tars (Yang et al., 2007). Overall, it can be concluded that xylan was responsible for CO release at lower temperature (below 400 °C) and cellulose was responsible for CO evolution at higher temperature (above 400 °C).

The evolution of CH_4 from all three components cellulose, xylan and lignin can be observed in Fig.17. The cracking of methoxyl groups (-O-CH_3) may be responsible for the formation of CH_4. In addition, the breaking of methylene groups may have partially increased the evolution of CH_4 (Liu et al., 2008). Xylan showed two CH_4 peaks at 305 °C and 553 °C. Primary pyrolysis may have contributed to the formation of CH_4 at 305 °C. The second peak at 553 °C could be due to the vapor phase secondary reactions at higher temperature. Cellulose and lignin produced low and high amounts of CH_4 respectively. The presence of methyl groups may be responsible for higher CH_4.

4. Conclusions:

The devolatilization of switchgrass, cellulose, xylan and lignin were carried out using TGA coupled with FTIR in nitrogen and air atmospheres. Significant weight loss of switchgrass occurred in the temperature range of 220-400 °C. The activation energy required for switchgrass decomposition was higher in air atmosphere (122.23 kJ mol^{-1}) as compared to activation energy in nitrogen atmosphere (103 kJ mol^{-1}). The kinetics

associated with cellulose, hemicellulose and lignin decompositions were considerably different. Cellulose decomposition required highest activation energy, whereas, lignin decomposition required lowest activation energy. Under oxidizing conditions, the activation energies of all the model components increased.

CO_2, CO, CH_4 plus some hydrocarbons were identified as major volatiles evolved during switchgrass decomposition. Hemicellulose was responsible for most of the CO_2 evolution and lignin was responsible for most of the CH_4 evolution. Both cellulose and hemicellulose decompositions led to higher CO compared to CO formed from lignin decomposition.

References

1 Klass, D. L. Biomass energy in North American policies. *Energy Policy* **23**, 1035-1048 (1995).
2 Hall, D. O. Biomass energy in industrialised countries - A view of the future. *For. Ecol. Manage.* **91**, 17-45 (1997).
3 Biagini, E., Barontini, F. & Tognotti, L. Devolatilization of Biomass Fuels and Biomass Components Studied by TG/FTIR Technique. *Ind. Eng. Chem. Res.* **45**, 4486-4493, doi:10.1021/ie0514049 (2006).
4 Keshwani, D. R. & Cheng, J. J. Switchgrass for bioethanol and other value-added applications: A review. *Bioresource Technology* **100**, 1515-1523 (2009).
5 Massé, D. *et al.* Methane yield from switchgrass harvested at different stages of development in Eastern Canada. *Bioresource Technology* **101**, 9536-9541 (2010).
6 Kumar, A., Wang, L., Dzenis, Y. A., Jones, D. D. & Hanna, M. A. Thermogravimetric characterization of corn stover as gasification and pyrolysis feedstock. *Biomass and Bioenergy* **32**, 460-467 (2008).
7 Jeguirim, M. & Trouvé, G. Pyrolysis characteristics and kinetics of Arundo donax using thermogravimetric analysis. *Bioresource Technology* **100**, 4026-4031 (2009).
8 Lee, S.-B. & Fasina, O. TG-FTIR analysis of switchgrass pyrolysis. *Journal of analytical and applied pyrolysis* **86**, 39-43, doi:10.1016/j.jaap.2009.04.002 (2009).
9 Miranda, R., Sosa_Blanco, C., Bustos-Martínez, D. & Vasile, C. Pyrolysis of textile wastes: I. Kinetics and yields. *Journal of Analytical and Applied Pyrolysis* **80**, 489-495 (2007).
10 Mani, T., Murugan, P., Abedi, J. & Mahinpey, N. Pyrolysis of wheat straw in a thermogravimetric analyzer: Effect of particle size and heating rate on devolatilization and estimation of global kinetics. *Chemical Engineering Research and Design* In Press, Corrected Proof (2010).
11 Branca, C., Albano, A. & Di Blasi, C. Critical evaluation of global mechanisms of wood devolatilization. *Thermochimica Acta* **429**, 133-141 (2005).
12 Mészáros, E., Várhegyi, G., Jakab, E. & Marosvölgyi, B. Thermogravimetric and Reaction Kinetic Analysis of Biomass Samples from an Energy Plantation. *Energy & Fuels* **18**, 497-507, doi:10.1021/ef034030+ (2004).
13 Wang, C., Wu, Y., Liu, Q., Yang, H. & Wang, F. Analysis of the behaviour of pollutant gas emissions during wheat straw/coal cofiring by TG–FTIR. *Fuel Processing Technology* **92**, 1037-1041, doi:10.1016/j.fuproc.2010.12.029 (2011).
14 Giuntoli, J., Arvelakis, S., Spliethoff, H., de Jong, W. & Verkooijen, A. H. M. Quantitative and Kinetic Thermogravimetric Fourier Transform Infrared (TG-FTIR) Study of Pyrolysis of Agricultural Residues: Influence of Different Pretreatments. *Energy & Fuels* **23**, 5695-5706, doi:10.1021/ef9005719 (2009).
15 Fu, P. *et al.* FTIR study of pyrolysis products evolving from typical agricultural residues. *Journal of analytical and applied pyrolysis* **88**, 117-123, doi:10.1016/j.jaap.2010.03.004 (2010).
16 Chouchene, A., Jeguirim, M., Khiari, B., Zagrouba, F. & Trouvé, G. Thermal degradation of olive solid waste: Influence of particle size and oxygen concentration. *Resources, Conservation and Recycling* **54**, 271-277 (2010).

17 Mani, T., Murugan, P., Abedi, J. & Mahinpey, N. Pyrolysis of wheat straw in a thermogravimetric analyzer: Effect of particle size and heating rate on devolatilization and estimation of global kinetics. *Chemical Engineering Research and Design* **88**, 952-958, doi:10.1016/j.cherd.2010.02.008 (2010).
18 Haykiri-Acma, H., Yaman, S. & Kucukbayrak, S. Effect of heating rate on the pyrolysis yields of rapeseed. *Renewable Energy* **31**, 803-810, doi:10.1016/j.renene.2005.03.013 (2006).
19 Al-Harahsheh, M. *et al.* Effect of demineralization and heating rate on the pyrolysis kinetics of Jordanian oil shales. *Fuel Processing Technology* **92**, 1805-1811, doi:10.1016/j.fuproc.2011.04.037 (2011).
20 Wang, L., Kumar, A., Hanna, M., Weller, C. L. & Jones, D. Thermal Degradation Kinetics of Distillers Grains and Solubles in Nitrogen and Air. *Energy Sources, Part A* **31**, 797-806 (2009).
21 Yan, R. *et al.* Influence of temperature on the distribution of gaseous products from pyrolyzing palm oil wastes. *Combustion and Flame* **142**, 24-32, doi:10.1016/j.combustflame.2005.02.005 (2005).
22 Orfão, J. J. M., Antunes, F. J. A. & Figueiredo, J. L. Pyrolysis kinetics of lignocellulosic materials—three independent reactions model. *Fuel* **78**, 349-358, doi:10.1016/s0016-2361(98)00156-2 (1999).
23 Carrier, M. *et al.* Thermogravimetric analysis as a new method to determine the lignocellulosic composition of biomass. *Biomass and Bioenergy* **35**, 298-307, doi:10.1016/j.biombioe.2010.08.067 (2011).
24 A. Sluiter, B. H., R. Ruiz, C. Scarlata, J. Sluiter, D. Templeton, and D. Crocker. Determination of Extractives in Biomass. (2008).
25 A. Sluiter, B. H., R. Ruiz, C. Scarlata, J. Sluiter, D. Templeton, and D. Crocker. Determination of Structural Carbohydrates and Lignin in Biomass. (2008).
26 Wiselogel, A. E. *et al.* Compositional changes during storage of large round switchgrass bales. *Bioresource Technology* **56**, 103-109 (1996).
27 Liu, L., Ye, X. P., Womac, A. R. & Sokhansanj, S. Variability of biomass chemical composition and rapid analysis using FT-NIR techniques. *Carbohydrate Polymers* **81**, 820-829 (2010).
28 Shen, D. K., Gu, S. & Bridgwater, A. V. Study on the pyrolytic behaviour of xylan-based hemicellulose using TG-FTIR and Py-GC-FTIR. *Journal of Analytical and Applied Pyrolysis* **87**, 199-206 (2010).
29 Biagini, E., Guerrini, L. & Nicolella, C. Development of a Variable Activation Energy Model for Biomass Devolatilization. *Energy & Fuels* **23**, 3300-3306, doi:10.1021/ef9001499 (2009).
30 Mansaray, K. G. & Ghaly, A. E. Determination of Reaction Kinetics of Rice Husks in Air Using Thermogravimetric Analysis. *Energy Sources, Part A: Recovery, Utilization, and Environmental Effects* **21**, 899 - 911 (1999).
31 Shafizadeh, F., McGinnis, G. D. & Philpot, C. W. Thermal degradation of xylan and related model compounds. *Carbohydrate Research* **25**, 23-33, doi:10.1016/s0008-6215(00)82742-1 (1972).
32 Yang, H. *et al.* Thermogravimetric Analysis−Fourier Transform Infrared Analysis of Palm Oil Waste Pyrolysis. *Energy & Fuels* **18**, 1814-1821, doi:10.1021/ef030193m (2004).

33 Vamvuka, D., Kakaras, E., Kastanaki, E. & Grammelis, P. Pyrolysis characteristics and kinetics of biomass residuals mixtures with lignite[small star, filled]. *Fuel* **82**, 1949-1960 (2003).
34 Kumar, V. *Pyrolysis and gasification of lignin and effect of alkali addition* Ph.D. thesis, Georgia Institute of Technology, (2009).
35 Munir, S., Daood, S. S., Nimmo, W., Cunliffe, A. M. & Gibbs, B. M. Thermal analysis and devolatilization kinetics of cotton stalk, sugar cane bagasse and shea meal under nitrogen and air atmospheres. *Bioresource Technology* **100**, 1413-1418, doi:10.1016/j.biortech.2008.07.065 (2009).
36 Zhang, X., Xu, M., Sun, R. & Sun, L. Study on Biomass Pyrolysis Kinetics. *Journal of Engineering for Gas Turbines and Power* **128**, 493-496 (2006).
37 Yang, H., Yan, R., Chen, H., Lee, D. H. & Zheng, C. Characteristics of hemicellulose, cellulose and lignin pyrolysis. *Fuel* **86**, 1781-1788, doi:10.1016/j.fuel.2006.12.013 (2007).
38 Fu, P. *et al.* Mechanism Study of Rice Straw Pyrolysis by Fourier Transform Infrared Technique. *Chinese Journal of Chemical Engineering* **17**, 522-529 (2009).
39 Li, S., Lyons-Hart, J., Banyasz, J. & Shafer, K. Real-time evolved gas analysis by FTIR method: an experimental study of cellulose pyrolysis. *Fuel* **80**, 1809-1817 (2001).
40 Shen, D. K. & Gu, S. The mechanism for thermal decomposition of cellulose and its main products. *Bioresource Technology* **100**, 6496-6504 (2009).
41 Liu, Q., Wang, S., Zheng, Y., Luo, Z. & Cen, K. Mechanism study of wood lignin pyrolysis by using TG-FTIR analysis. *Journal of Analytical and Applied Pyrolysis* **82**, 170-177 (2008).

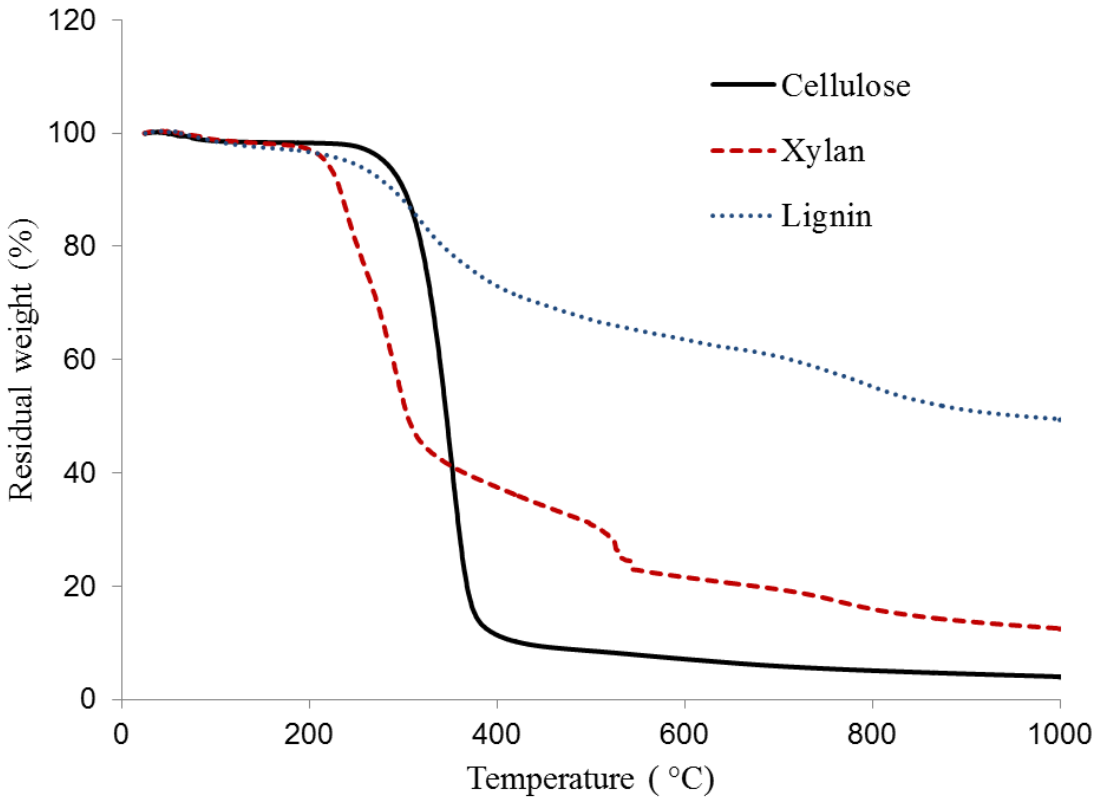

Figure 1. Weight loss profile of cellulose, xylan and lignin in nitrogen atmosphere at a heating rate of 50 °C min^{-1}

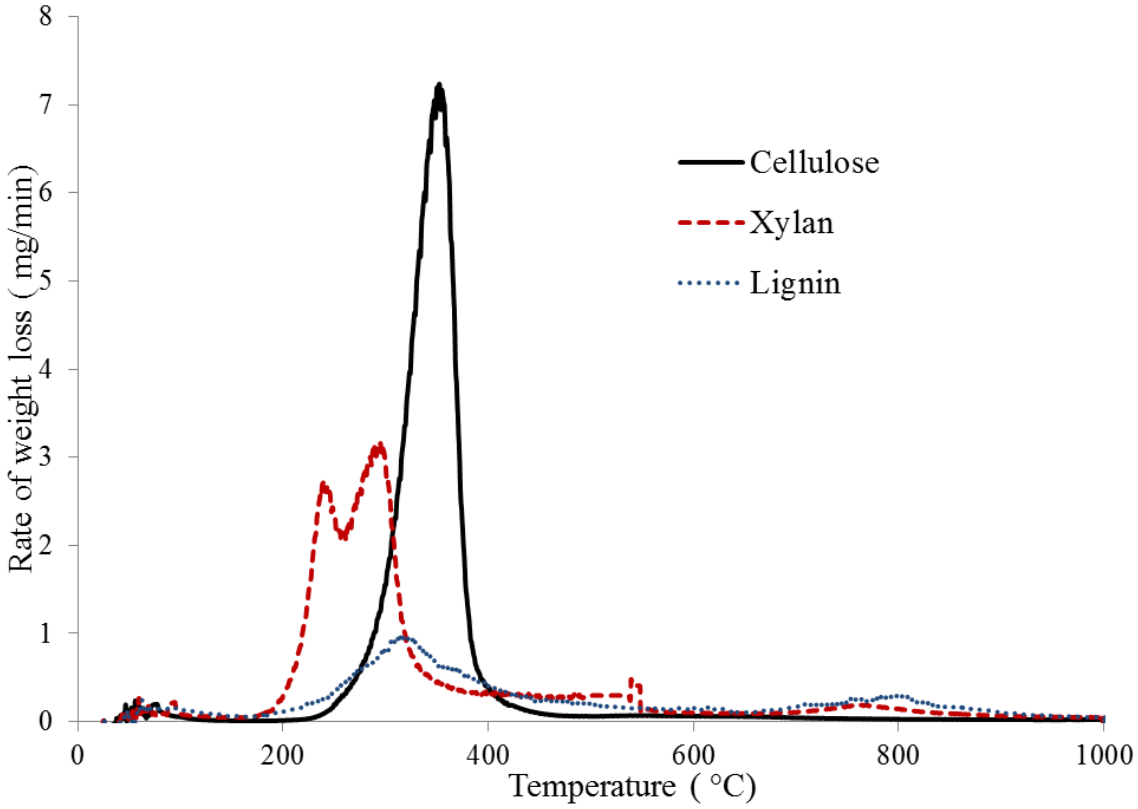

Figure 2. Rate of weight loss profile of cellulose, xylan and lignin in nitrogen atmosphere at a heating rate of 50 °C min^{-1}

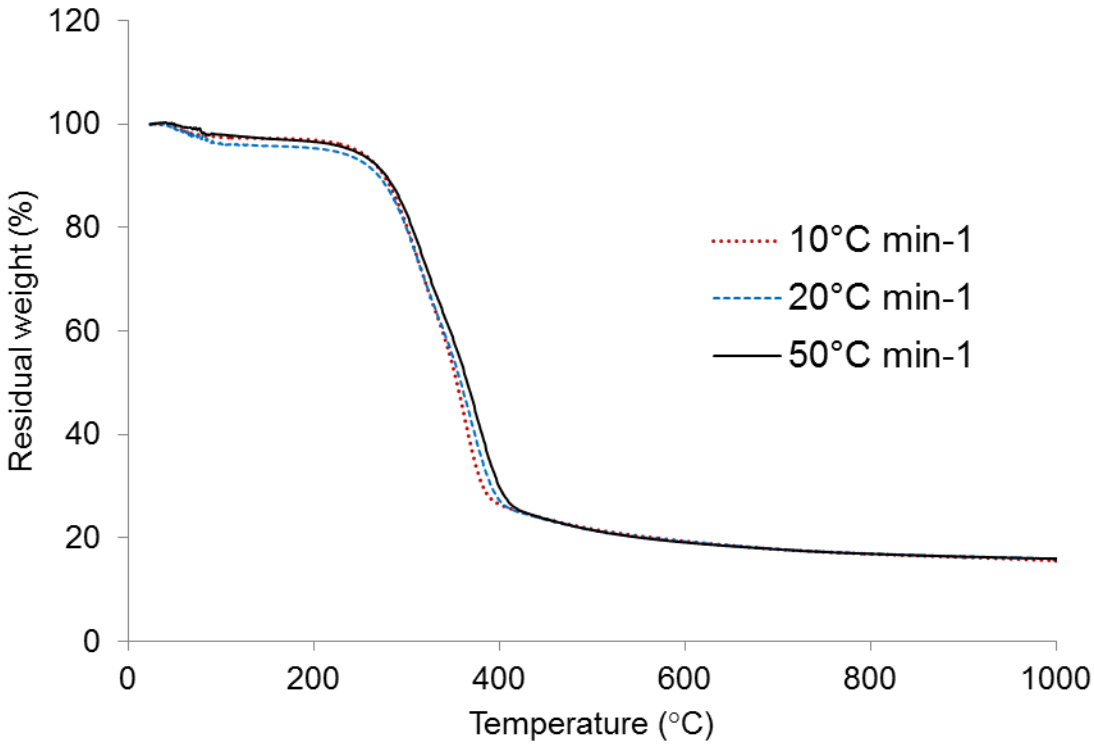

Figure 3. Weight loss profile of switchgrass at three heating rates in nitrogen atmosphere

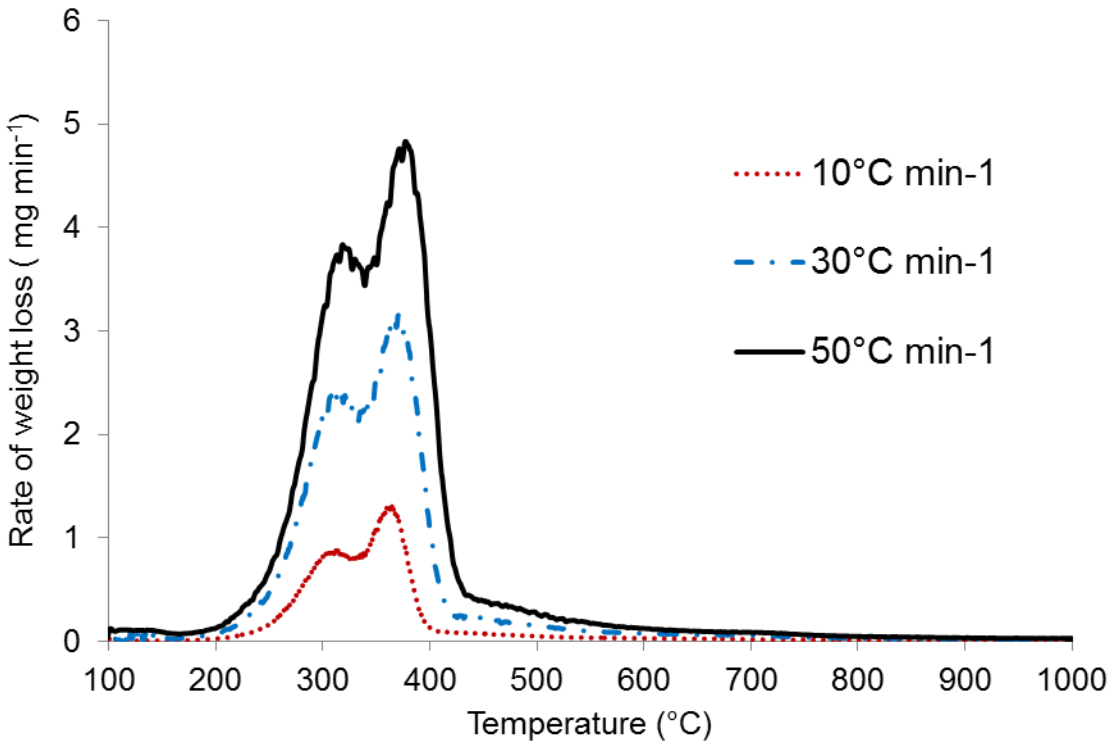

Figure 4. Rate of weight loss profile of switchgrass at three heating rates in nitrogen atmosphere

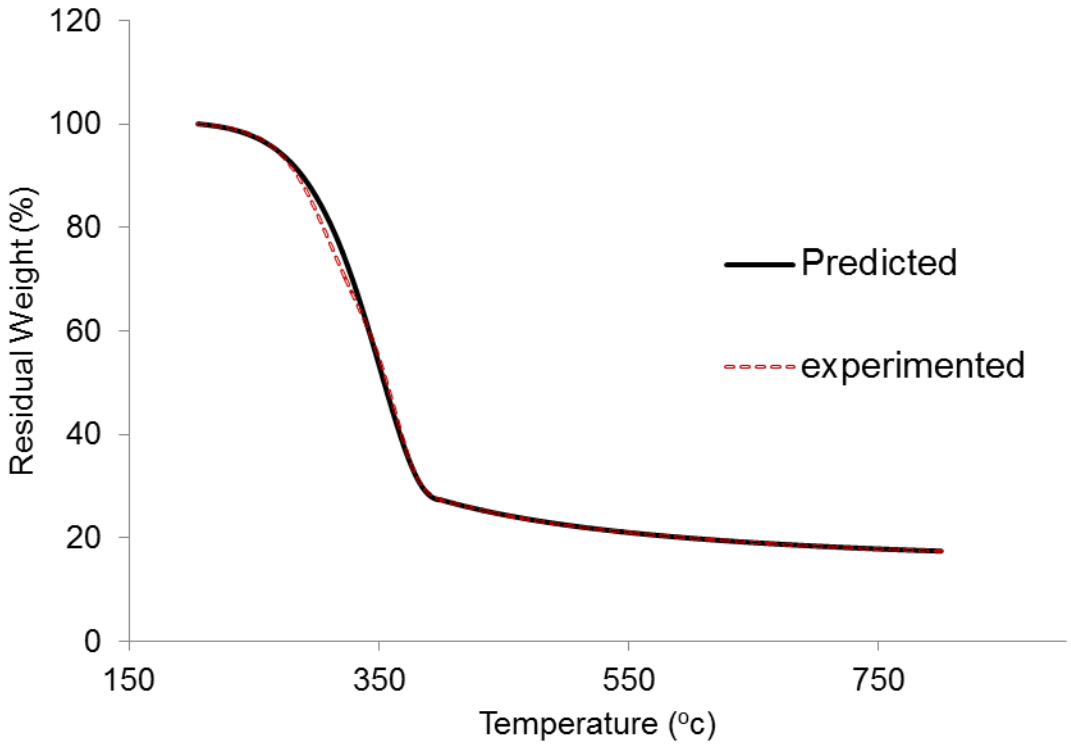

Figure 5. Comparison of predicted data with experimental data during second stage and third stage decompositions in nitrogen atmosphere

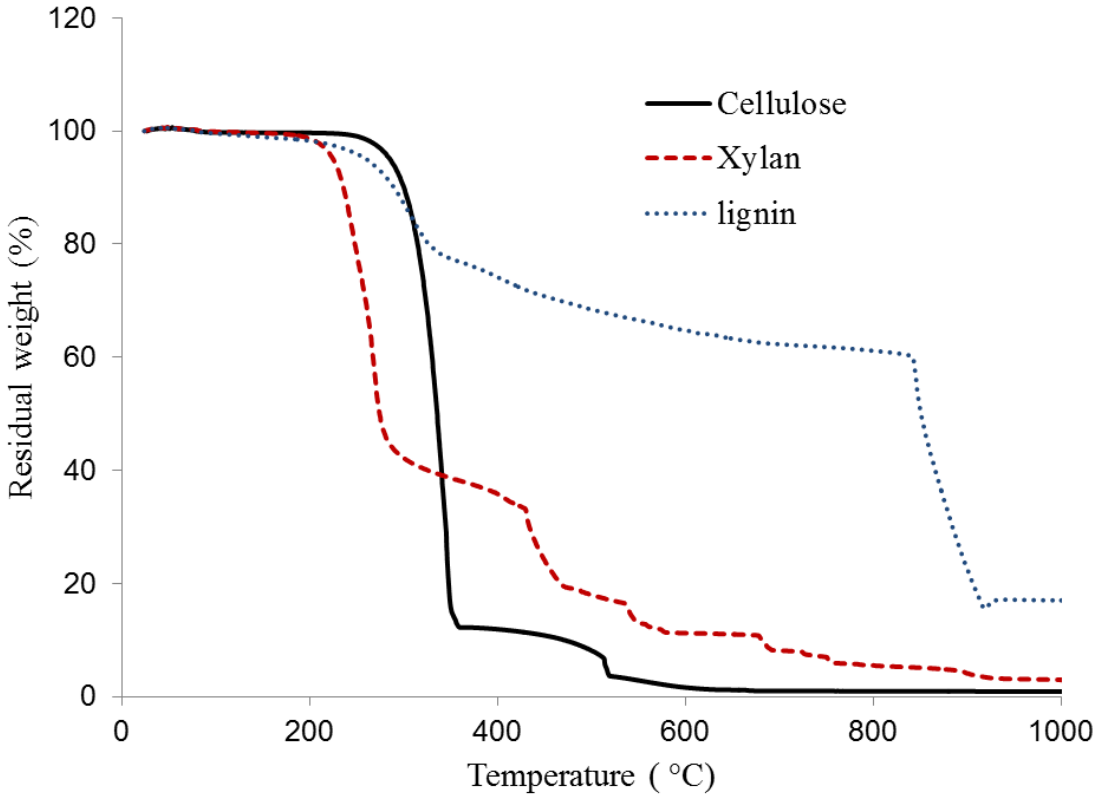

Figure 6. Weight loss profile of cellulose, xylan and lignin in air atmosphere at a heating rate of 50 °C min^{-1}

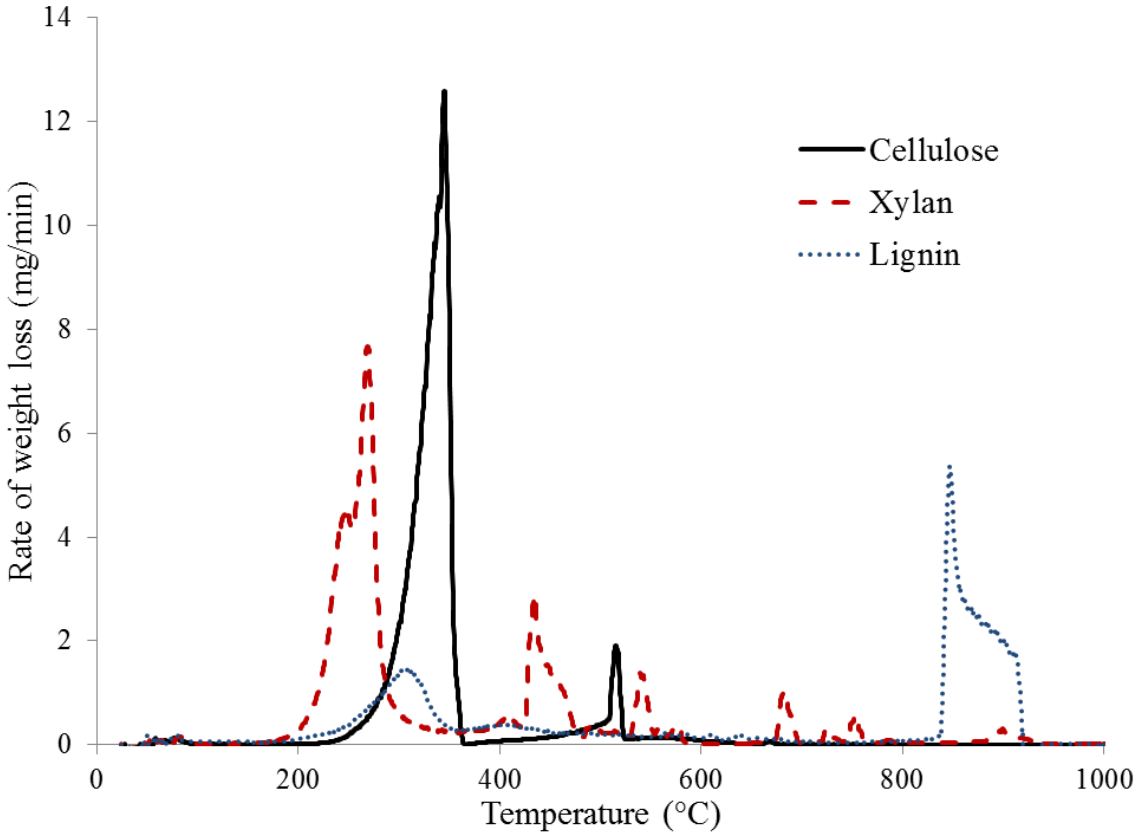

Figure 7. Rate of weight loss profile of cellulose, xylan and lignin in air atmosphere at a heating rate of 50 °C min^{-1}

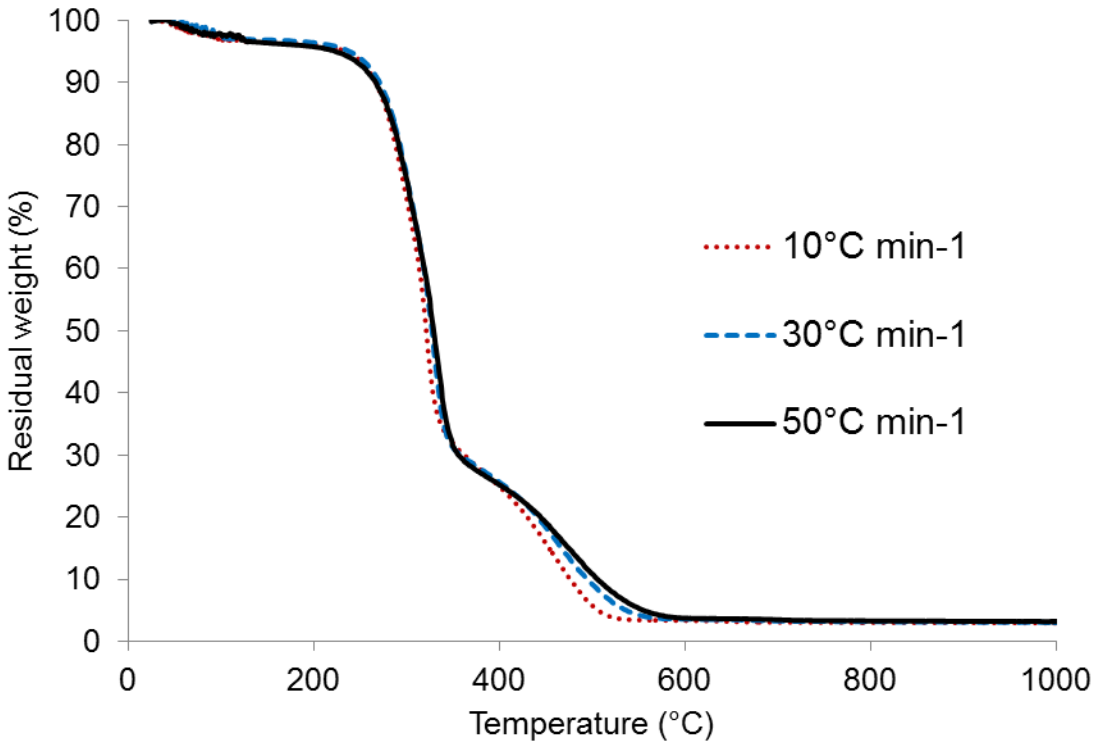

Figure 8. Weight loss of switchgrass at three heating rates in air atmosphere

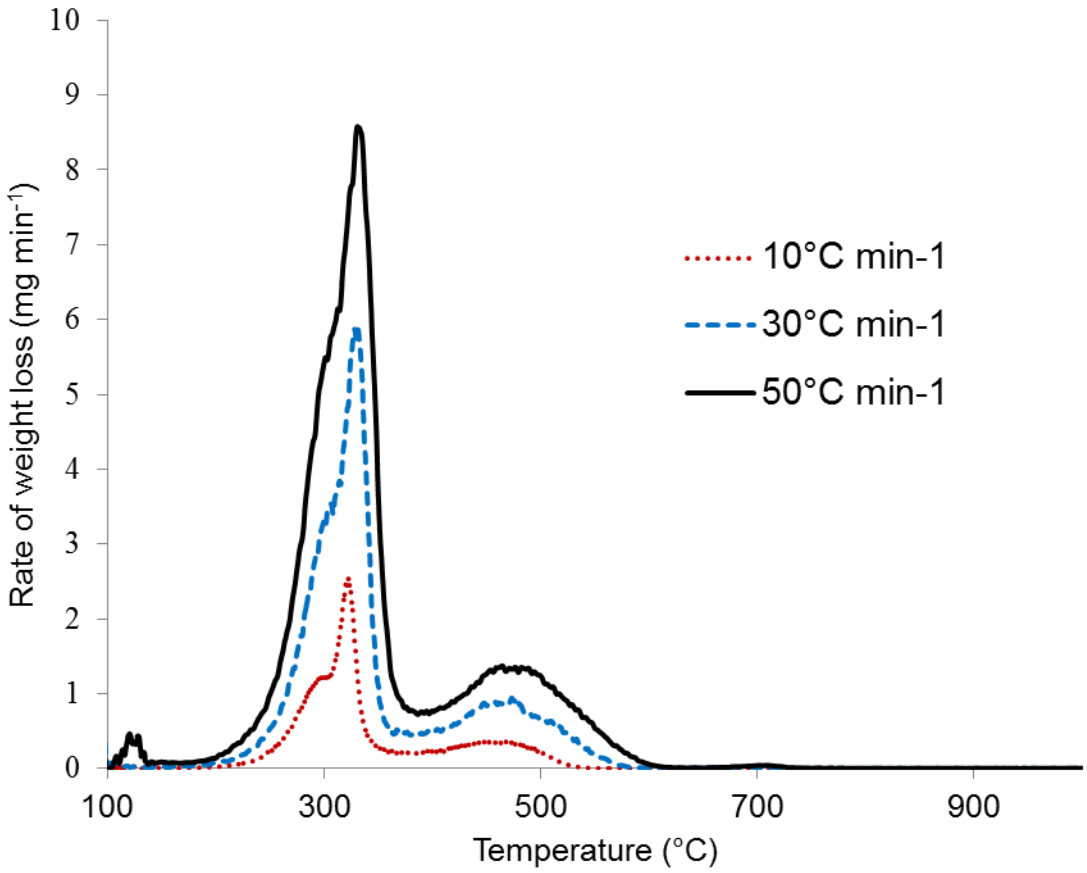

Figure 9. Rate of weight loss of switchgrass at three heating rates in air atmosphere

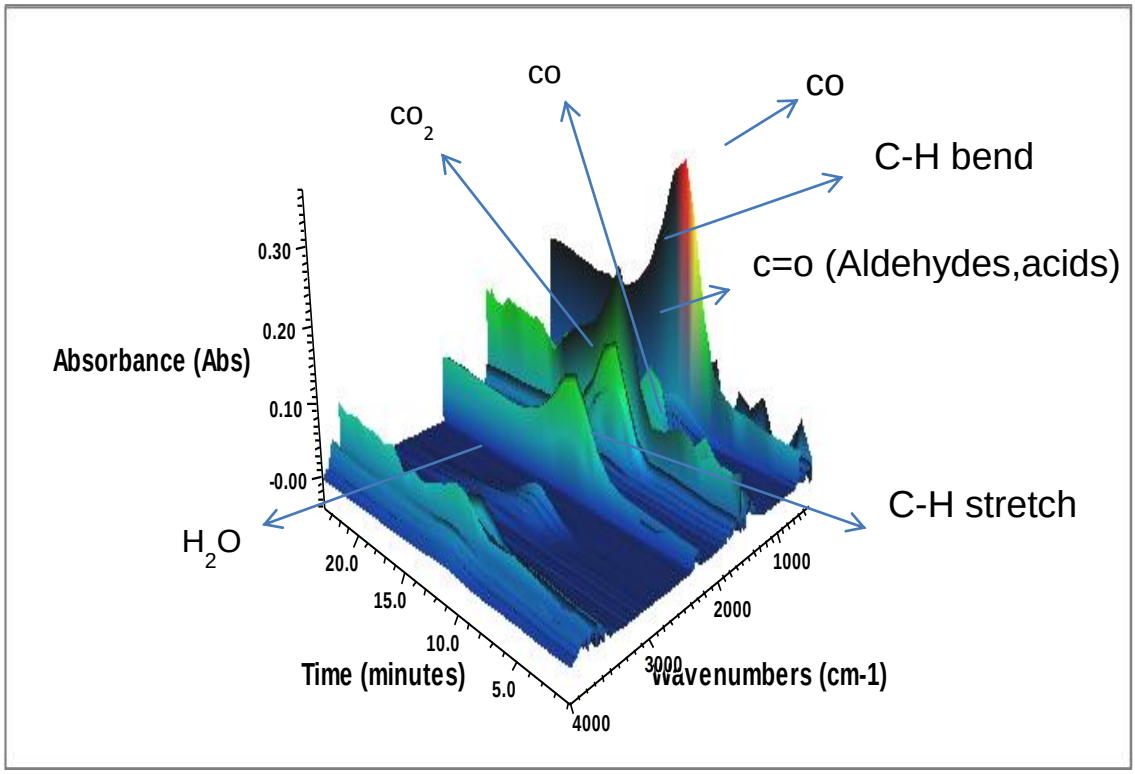

Figure 10. Infrared stack profile of volatiles evolved during switchgrass decomposition in nitrogen atmosphere

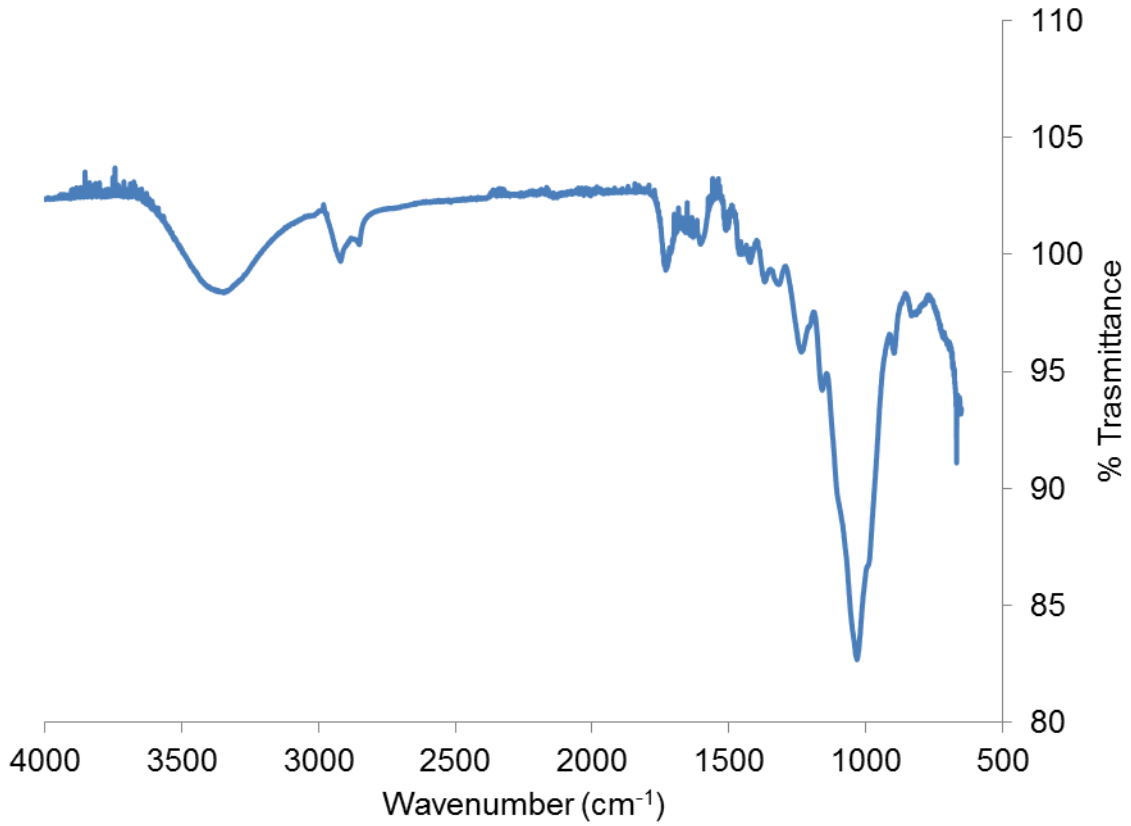

Figure 11. Chemical structure of switchgrass using FTIR

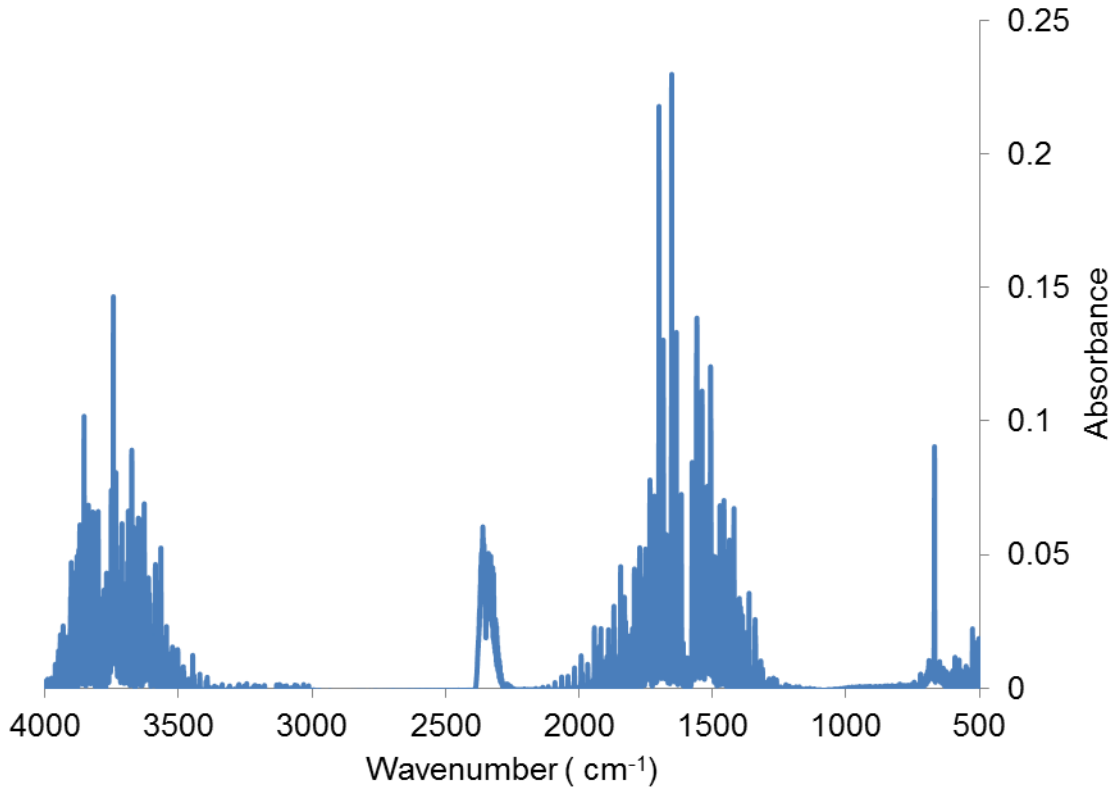

Figure 12. FTIR profile of gases evolved during switchgrass decomposition at 115 °C in nitrogen atmosphere

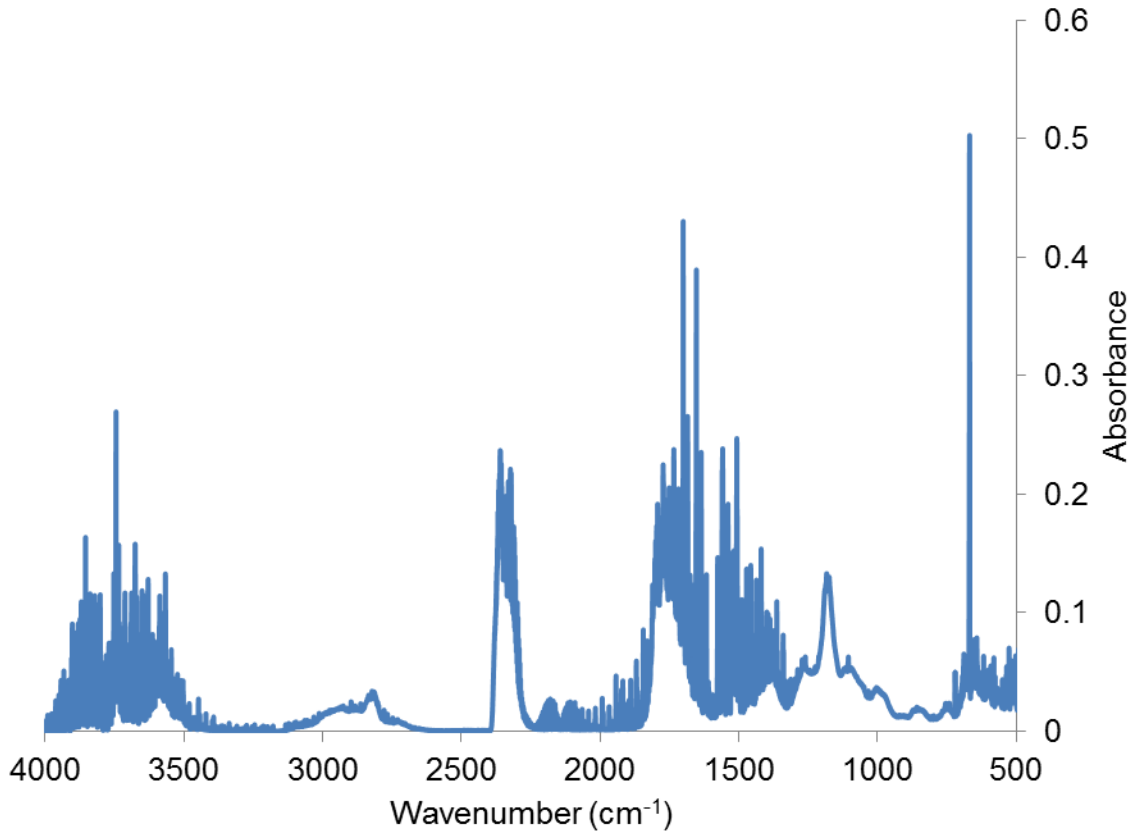

Figure 13. FTIR profile of gases evolved during switchgrass decomposition at 367 °C in nitrogen atmosphere

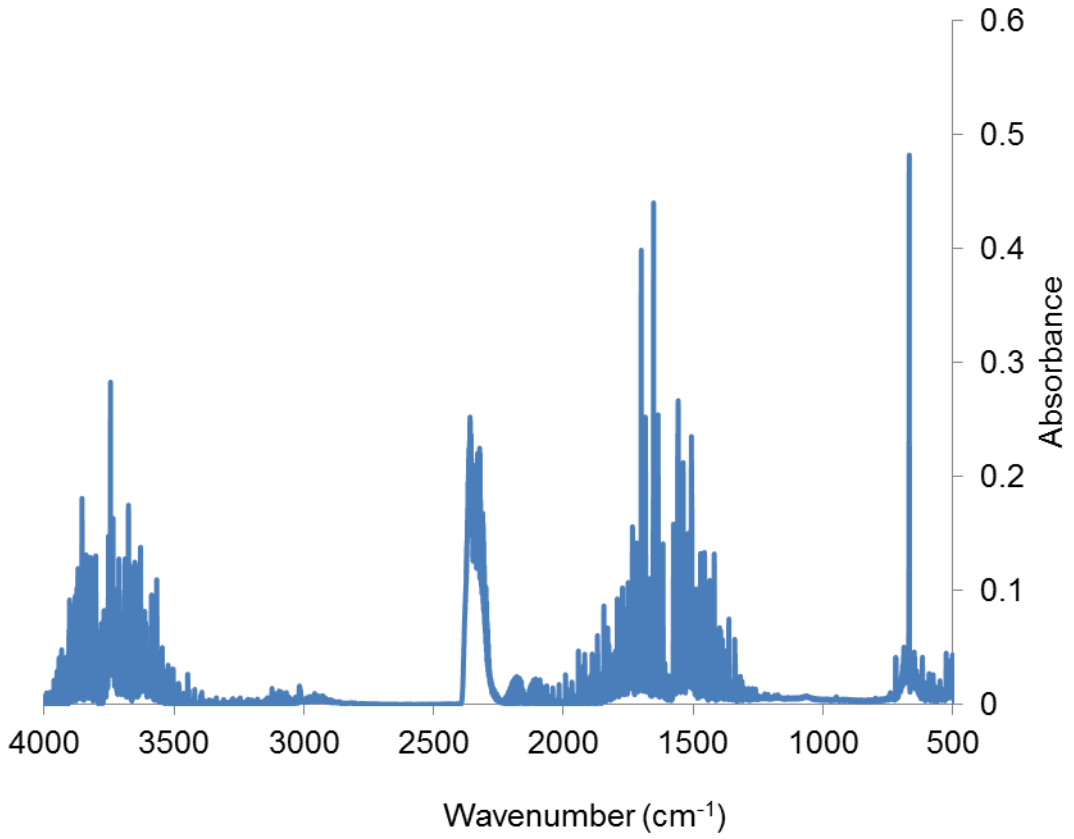

Figure 14. FTIR profile of gases evolved during switchgrass decomposition at 590 °C in nitrogen atmosphere

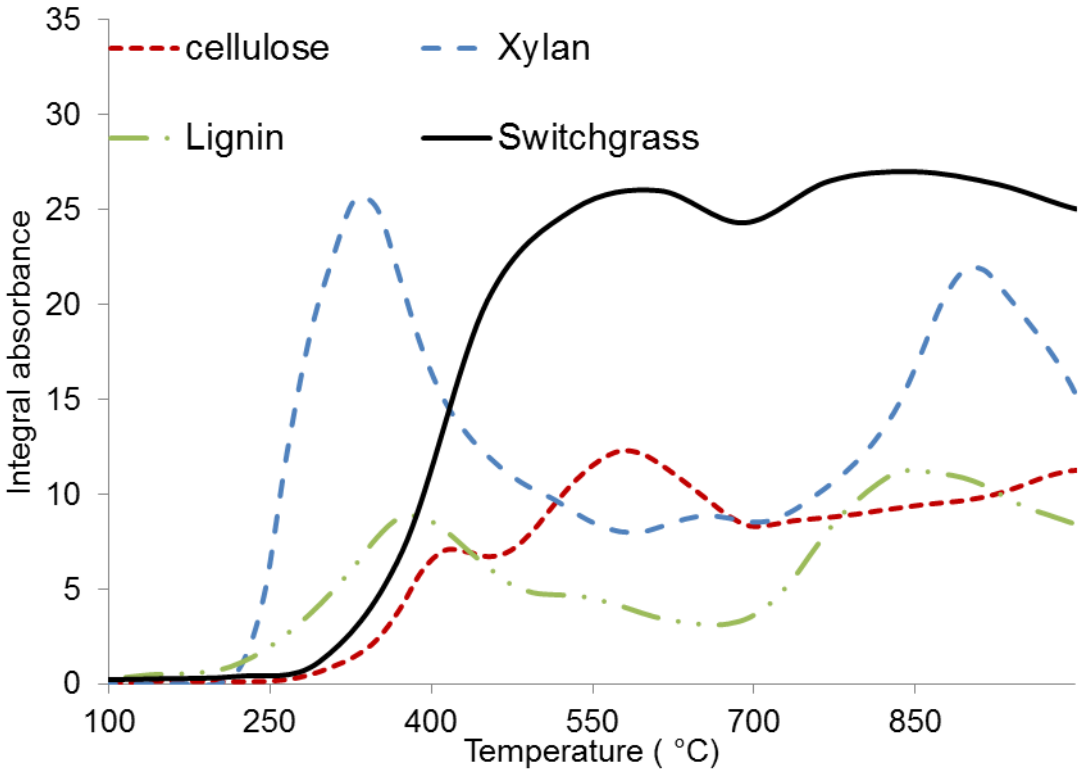

Figure 15. CO_2 evolved during decomposition of switchgrass and its model components in nitrogen atmosphere

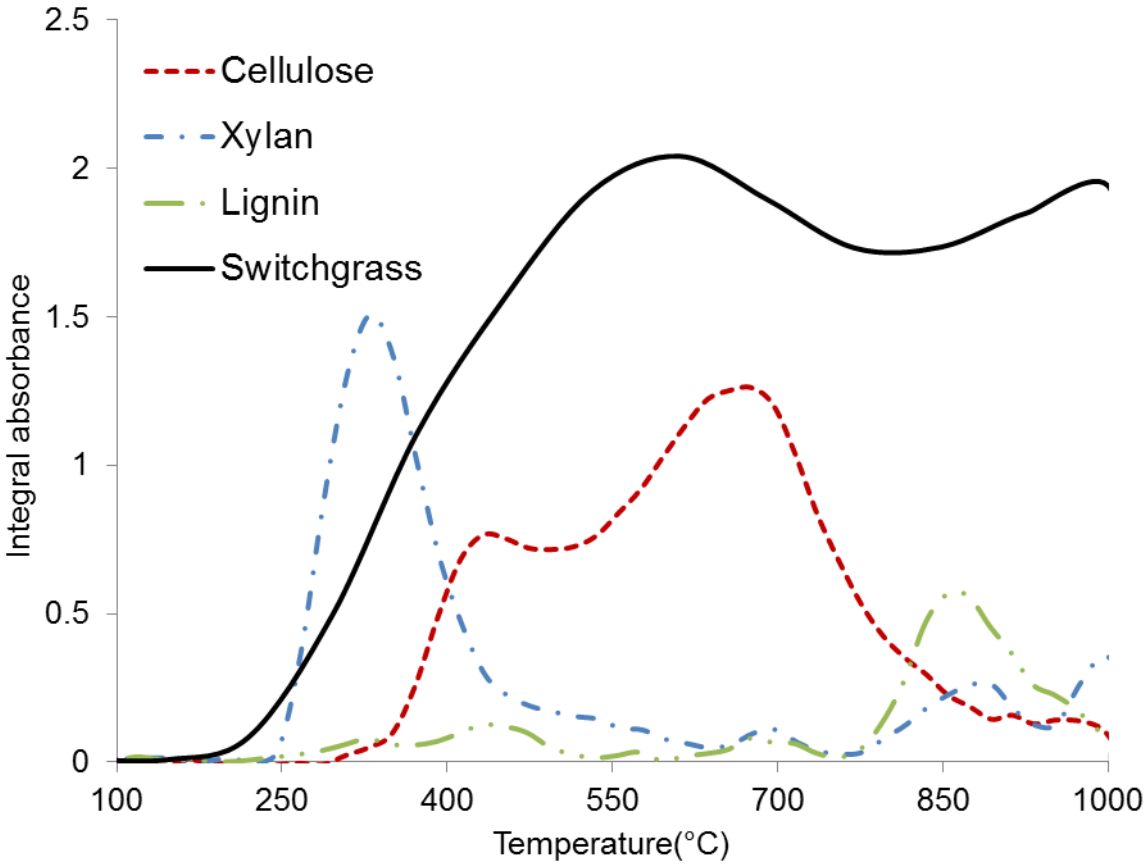

Figure 16. CO evolved during decomposition of switchgrass and its model components in nitrogen atmosphere

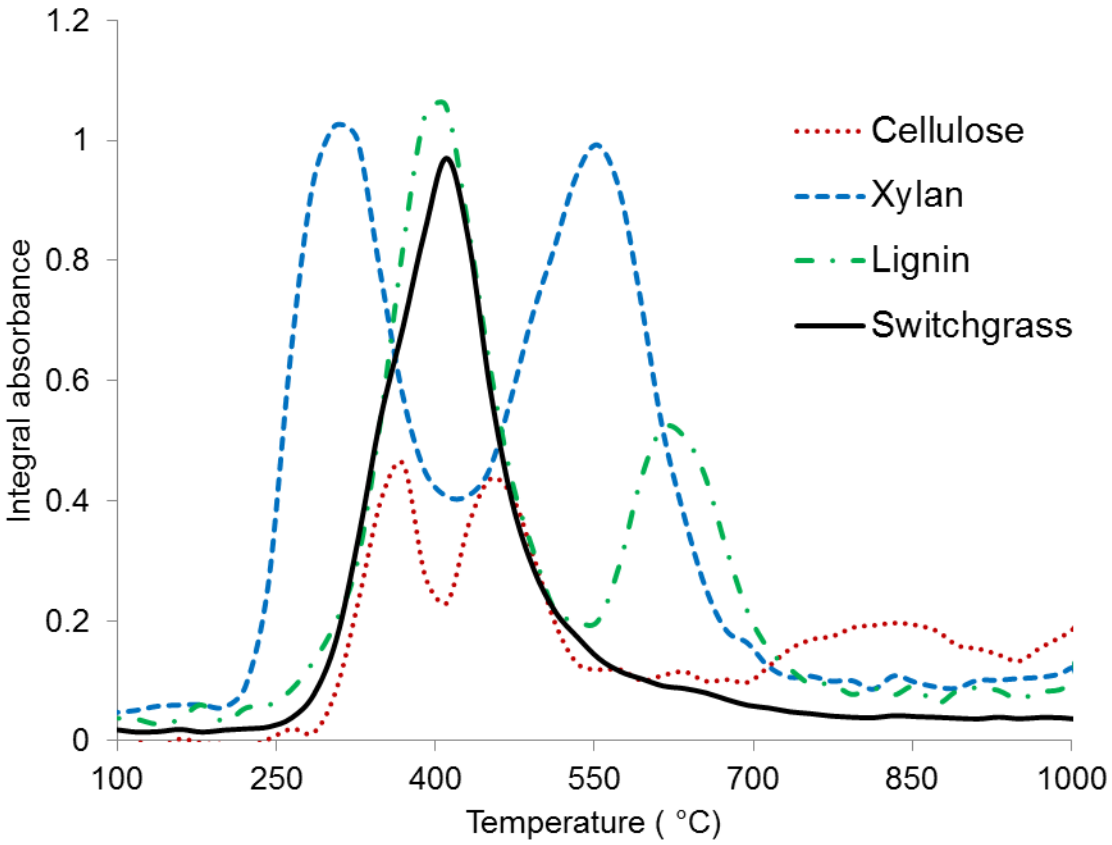

Figure 17. CH_4 evolved during decomposition of switchgrass and its components in nitrogen atmosphere

Table 1. Ultimate and proximate analyses of switchgrass

Ultimate analysis (%dry)				Proximate analysis (%dry)			
				In Nitrogen		In Air	
C	H	N	O	Volatiles	Fixed carbon+ ash	Volatiles	Ash
46.62	5.74	0.18	42.27	79.72±0.93	15.94±0.21	93.72±0.13	3.02±0.18

Table 2. Chemical composition of switchgrass

Switchgrass components (% dry)	Current study	Wiselogel et al. (1996)	Liu and Ye (2010)
Glucan	38.46±0.69	37.8±1.3	39.31±0.12
xylan	26.34±0.54	24.9±0.7	22.67±0.19
Galactan	1.16±0.18	1.1±0.1	1.81±0.12
Aribinana	3.41±0.32	3.4±0.1	3.17±0.03
Mannan	0.13±0.22	0.4±0.1	1.03±0.10
Lignin	21.40±0.24	21.4±0.2	21.36±0.12
Ash	1.91±0.095		1.60±0.07

Table 3. Weight loss kinetic parameters of switchgrass and its components in nitrogen atmosphere

Sample	T (°C)	E(kJ mol^{-1})	A	n	R^2
Switchgrass	220-400	103.7	2.16×10^{7}	0.67	0.95
Cellulose	270-390	119.21	6.86×10^{9}	0.77	0.94
Xylan	200-260	116.84	5.4×10^{11}	0.44	0.95
	260-315	58.48	1.66×10^{5}	0.40	0.94
Lignin	200-400	43.29	1.4×10^{3}	0.54	0.92
	680-740	98.06	5.5×10^{4}	0.07	0.92

Table 4. Weight loss kinetics parameters of weight loss of switchgrass and its components in air atmosphere

Sample	T (°C)	E(kJ mol^{-1})	A(s^{-1})	n	R^2
Switchgrass	220-345	122.23	3.88×10^{10}	0.52	0.99
Cellulose	250-360	135.21	2.73×10^{11}	0.77	0.97
Xylan	200-280	118.54	3.10×10^{11}	0.47	0.97
Lignin	200-340	67.62	5.80×10^{5}	0.50	0.96
	840-915	160.15	1.32×10^{-8}	0.03	0.86

CHAPTER III

Effects of cellulose, hemicellulose and lignin on thermochemical conversion characteristics of the selected biomass

Abstract:

The objective of this study was to investigate effects of biomass constituents (cellulose, hemicellulose and lignin) on biomass thermal decomposition and gas evolution profiles of four biomass materials. Switchgrass, wheat straw, eastern redcedar and dry distilled grains with solubles (DDGS) were selected as the biomass materials. No significant difference was observed in the weight loss profiles of switchgrass, wheat straw and eastern redcedar even though their cellulose, hemicellulose and lignin contents were considerably different. The weight loss kinetic parameters were also not significantly different except for activation energy of the eastern redcedar. However, biomass composition did significantly affect gas evolution profiles. The higher contents of cellulose and hemicellulose in switchgrass and wheat straw may have resulted in their higher CO and CO_2 concentrations as compared to eastern redcedar. On the other hand, higher lignin content in eastern redcedar may have resulted in significantly its high CH_4 concentration.

Keywords: Biomass; thermochemical conversion; thermal degradation; product yields.

1. Introduction:

The rapid increase in fossil fuels consumption coupled with concerns over fossil fuel reserves have motivated exploration of sustainable energy sources (Hill et al., 2006). Biomass is considered as one of the potential sustainable energy sources and its utilization is gaining increased momentum because of its wide availability and environmentally-friendly nature (Tilman et al., 2006). Various technologies have been developed over the years to convert biomass into other more valuable forms of energy. Thermochemical conversion technologies, such as gasification and pyrolysis, hold promise because these are flexible in accepting a wide range of feedstocks and also producing a wide range of products with high efficiencies (Bridgwater, 2006). During thermochemical processes, heat is applied to break the biomass into desirable products. The efficiency of thermochemical conversions depend on many factors such as feedstock properties, reactor design and reaction conditions (Lettner et al., 2007). Extensive research has been conducted to understand the effects of operating parameters such as temperature, heating rate and residence time on products during the thermochemical conversions (Demirbas, 2001; Demirbas, 2004; Goyal et al., 2008; Kumar et al., 2009a). Different reactor configurations have evolved to enhance the process efficiency by improving heat and mass transfers within the reactor (Meier & Faix, 1999). Researchers have also studied the effect of physical properties, such as particle size and shape, on products of thermochemical conversion (Bridgwater, 1999; Goyal et al., 2008; Ryu et al., 2006). However, studies on the effect of major biomass components, such as cellulose, hemicellulose and lignin on gaseous products from

thermochemical conversion are limited in literature. Biomass such as energy crops, agricultural residues, and woody materials have widely been used as feedstocks for gasification and pyrolysis. The biomass feedstocks contain different amounts of cellulose, hemicellulose and lignin. Their polymer structure and length, and their cross-linkage vary substantially, resulting in different thermal decomposition characteristics and products during gasification and pyrolysis. For biorefineries to be feedstock flexible, understanding the effects of the major biomass components, cellulose, hemicellulose and lignin, on thermal decomposition of biomass and resulting products is crucial.

Typically, cellulose, hemicellulose and lignin constitute about 85-90 % of lignocellulosic biomass; organic extractives and inorganic minerals constitute the rest. Cellulose is the major structural polymer of a plant cell wall and usually exists as long thread like fibers called microfibrils. It is a linear polysaccharide consisting of monomeric units of anhydro-D-glucose units with a β-(1→4)-linkage (Mohan et al., 2006; Pérez et al., 2002). This nature of bonding allows the microfibril structure to develop strong inter-molecular and intra-molecular hydrogen bonding (Keshwani, 2010). Microfibrils are usually embedded on a matrix that contains hemicellulose and lignin. Hemicellulose is a branched polysaccharide comprised of different sugar monomers such as glucose, xylose, mannose, galactose and arabinose and uronic acids (Bidlack et al., 1992; Pérez et al., 2002). Unlike cellulose, they do not form microfibrils. But, they can form hydrogen bonds with the cellulose and lignin and hence they are referred as "cross linking glucans." Lignin is the cementing material that provides elasticity and mechanical strength to the wood (Wang et al., 2011). It is a phenolic macromolecule with a high degree of cross linking between the phenylpropane units.

This cross linking makes lignin more thermally stable than hemicellulose (Ramiah, 1970). The difference in reactivity of biomass due to the variations in chemical composition must be better understood so that process can be optimized to obtain fuels and chemicals with high selectivity and efficiency (Carrier et al., 2011).

The chemical composition and nature of the biomass polymers differ significantly with biomass types. On a dry basis, softwoods contain 40-50% wt. cellulose, 25-35% wt. hemicellulose and 16-33% wt. lignin (Mohan et al., 2006). Softwoods contain more lignin but less hemicellulose as compared to agricultural residues or herbaceous crops. Agricultural residues, such as corn stover, consist of 33-35 % wt. cellulose, 21-24 % wt. hemicellulose and 17-22 % wt. lignin (Johnson et al., 1994). Herbaceous crops, such as switchgrass, contain much higher cellulose (38-40 % wt.) and lower lignin content (15-19 % wt.) than those in softwoods (Jefferson et al., 2004; Lee & Owens, 2005). Harvesting technique and biomass storage also affects biomass composition (Johnson et al., 1994; Mulkey & Lee, 2006). To utilize the biomass feedstocks with wide variability in composition, it is imperative that effects of the primary constituents, i.e. cellulose, hemicellulose and lignin, on the thermochemical process and their contribution in resulted products be better understood.

Thermogravimetric analysis (TGA) is a widely used technique to obtain precise weight loss profile during biomass thermal decomposition (Evans & Milne, 1987; Ghetti et al., 1996; Kumar et al., 2008b; Mani et al., 2010b). Fourier Transform Infrared Spectrometry (FTIR) and Mass Spectrometry (MS) are two well-known techniques for online gas analysis (Xie & Pan, 2001). In this study, TGA was used to study weight loss characteristics and FTIR-MS were used for online gas analysis. Raveendran et al. (1996)

studied the thermal degradation properties of rice husk, rice straw and corn stock. Pyrolysis kinetic characteristics of olive residue and sugar cane bagasse were investigated using thermogravimetric technique by Ounas et al. (2011). However, there is limited information available on how different biomass components contribute to weight-loss profiles and product gas evolution profiles during thermochemical conversion processes. The present study specifically focuses on comparing and contrasting biomass based on their compositions and analyzing their effects on weight-loss and product evolution patterns during thermochemical conversions.

2 Materials and Methods:

2.1 Materials

Switchgrass (SG), wheat straw (WS), eastern redcedar (ER) and dried distilled grains with solubles (DDGS) were the biomass feedstocks used in this study. Four biomass types were represented by these feedstocks. Switchgrass is an herbaceous crop, wheat straw is an agricultural residue, eastern redcedar is a woody biomass and DDGS is a byproduct from corn dry milling ethanol production process. For compositional analysis and weight-loss study, all biomass were ground to pass through a 2 mm screen in a Thomas-Willey mill (Arthur H. Thomas Co., Philadelphia). The small particle size was needed to reduce heat and mass transfer limitations during their thermal decompositions. Avicel PH 105 Cellulose (FMC Biopolymer, Philadelphia), beech wood xylan (Sigma Aldrich, St. Louis) and alkali lignin (Sigma Aldrich, St. Louis) were used as models of cellulose, hemicellulose and lignin, respectively. Ultimate analyses for all

biomass and model components, shown in Table 1, were performed by Midwest Microlab, LLC (Indianapolis, IN).

2.2. Determination of chemical composition of biomass:

For compositional analysis, biomass sample was sieved through +60/+400 (250 µm/38 µm sieve openings) sieve plates on a horizontal sieve shaker according to National Renewable Energy Laboratory (NREL) procedures (Carrier et al., 2011). About 200 g of the sample was loaded into the sieve. More than 95% of the biomass was retained on +60 sieve plate. Biomass retained on this plate was used for extraction and compositional analysis. Water and ethanol extraction of biomass was carried using an accelerated solvent extractor (ASE) (Model 300, Dionex Corporation, Sunnyvale, CA) to remove the non-structural material using NREL protocols (A. Sluiter, 2008a). The weight of extractives was recorded after air drying.

Following extraction, the residual material was analyzed for structural carbohydrates, lignin, acetyl content and ash content using the two step acid hydrolysis procedure developed by NREL (A. Sluiter, 2008b; Mani et al., 2010b). For ash analysis and determination of acid insoluble lignin (AIL), a muffle furnace (Fisher Scientific, Dubuque, IA) was used. Structural carbohydrates were analyzed using a HPLC (Model 1100, Agilent Technologies, Santa Clara, CA) connected to a refractive index detector (RID) with an Bio-Rad Aminex HPX-87P column (Bio-Rad, Sunnyvale, CA). Deionized water was used as an eluent at a flow rate of 0.6 ml/min. The column was maintained at 85 °C. The total run time using this column was 30 min. The HPLC with Chemstation software (Agilent Technologies) was calibrated at five levels using known concentrations of compounds before being used to quantify the concentration of

compounds. Acid soluble lignin (ASL) content of biomass was determined using a UV-Vis spectrophotometer (Cary 50 Bio, Varian Inc., Palo Alto, CA, USA) at a wavelength of 205 nm and an extinction coefficient of 110 L/g-cm. The chemical compositions of switchgrass, wheat straw, eastern redcedar and DDGS, determine using above procedure, are shown in Table 2.

2.3 Experimental setup:

A thermogravimetric analyzer (Versa Therm, ThermoFischer Scientific, MA, USA) was used for studying the biomass thermal decomposition. The initial weight of biomass used in the study was 50±0.5 mg. Argon was used as non-oxidizing agent with a flow rate of 60 ml/min. The temperature range for decomposition was 25-1000 °C with a ramping rate of 80 °C min^{-1}. Fourier Transform Infrared Spectrometry (Nicolet 6700, ThermoFischer Scientific, USA) and Mass Spectrophotometer (Agilent 7890A, Agilent Technologies) were used for online gas analysis. FTIR was connected to the TGA through a transfer line that was maintained at 300 °C to avoid condensation of volatiles. To avoid the entry of volatiles into the MS, a cold trap was set up using ethanol and ice between FTIR and MS. FTIR was calibrated to quantify CO,CO_2 and CH_4; whereas, MS was calibrated to quantify the argon gas.

2.4 Determination of reaction kinetics parameters

Several approaches have been reported to determine the kinetic parameters such as activation energy, pre-exponential factor and order of the reaction for biomass decomposition. Since thermochemical processes involve many complex reactions, no single model can adequately represent the reaction kinetics of a variety of biomass

(Biagini et al., 2006). The kinetic model used in this study is based on the Arrhenius equation. This model was successfully used by Kumar et al. (2008a) for corn stover, Chouchene et al. (2010) for olive waste and Mansaray and Ghaly (1999) for rice husk. The weight-loss kinetic parameters were determined using the following rate equation.

$$-\frac{dX}{dt} = kX^n \quad (1)$$

where, n is the order of the reaction, and X is the weight of the sample (mg).

The reaction constant (k) based on Arrhenius equation can be written as,

$$k = A\, e^{-E/RT} \quad (2)$$

where, n is the order of the reaction, A is the pre exponential factor (S^{-1}), E is the activation energy (kJ mol^{-1}), T is the temperature (K) and R is the universal gas constant (mol^{-1} K^{-1}).

A multi-linear regression technique was applied on the linearized form of the Arrhenius equation to determine the reaction kinetic parameters. The simplified rate equation is shown below.

$$y = a + bx + cz \quad (3)$$

where,

$$y = ln\left[\frac{1}{w_f - w_i}\frac{dw}{dt}\right], x = \frac{1}{T}, z = ln\left(\frac{w - w_f}{w_i - w_f}\right),$$

$$a = ln(A), b = \left(\frac{-E}{R}\right), c = n$$

w is the sample weight at time t (mg),

w_i is the initial sample weight (mg),

w_f is the residual sample weight (mg)

2.5 Statistical Analysis

Analysis of variance for weight loss profiles was performed using repeated measures design in SAS Release 9.2 (SAS, Cary, NC, USA). Since weight loss and gas absorbance were measured over a range of temperature, temperature was considered as a factor in the treatment structure. A repeated measure analysis allowed finding the main effects of biomass type and temperature, and an interaction effect between biomass type and temperature. To analyze the effect of biomass type on gas evolution, post-hoc analysis was performed by comparing the means of gas absorbance for different biomass types using Fisher's Least Significant Difference (LSD) at α = 0.05 and GLM procedure.

3. Results and Discussion:

3.1 Weight loss characteristics of selected biomass:

The weight loss profile provided the instantaneous biomass weight at specific temperatures as biomass temperature was increased. Weight loss profiles for various biomass tested over temperature are shown in Fig. 1. Although the switchgrass, wheat straw and eastern redcedar contained different percentages of cellulose, hemicellulose and lignin, there was no statistical difference in their weight loss profiles ($p=0.9997$). However, as expected, there was a significant effect of temperature ($p<0.0001$) on the weight-loss profile due to the thermal decomposition of the samples. No interaction

between temperature and biomass type was observed. The weight loss profiles obtained in this study are consistent similar study done on bamboo, corn cobs, corn stalk and coconut shell (Al-Harahsheh et al., 2011; Singh et al., 2012).

Thermal decomposition of biomass occurred in three stages. First stage of the decomposition occurred in the temperature range of 25-125 °C and corresponded to the moisture evaporation. Second stage of the decomposition contributed to a major weight loss (60-70% wt.) in the temperature range of 200-400 °C. The major weight loss stage was due to the decomposition of primarily cellulose and hemicellulose in the biomass (Jeguirim & Trouvé, 2009). This was further confirmed by comparing with weight loss profiles of model components, cellulose and hemicellulose (Fig. 2). The figure shows that major portions of these two polysaccharides decomposed in the temperature range of 200-400 °C. Approximately 65-70% weight loss of switchgrass, wheat straw and redcedar occurred in this stage. The final stage of the decomposition occurred in the temperature range of 400-800 °C accounting for the remaining weight loss (approximately 10-12% wt.) in the sample weight.

Unlike biomass materials, model components (cellulose, hemicellulose and lignin) resulted in statistically different weight loss profiles ($p<0.0001$) as shown in the (Fig. 2). A interaction effect between model components and temperature was also significant ($p=0.0057$). Cellulose and hemicellulose had approximately 90% (wt) and 70% (wt) weight loss within narrow temperature ranges of 250-360 °C and 200-280 °C, respectively. On the other hand, lignin had a total of only 60% weight loss. Interestingly, even though redcedar had higher lignin content, its total weight loss at the end of decomposition was comparable with switchgrass and wheat straw. Higher than expected

weight loss (conversion) could be due to the catalytic effects of char and ash generated from decompositions of cellulose and hemicellulose in eastern redcedar.

The weight loss rates of switchgrass, wheat straw and redcedar were also no different, except of an additional shoulder peak in switchgrass weight loss rate (Fig. 3). The shoulder peak may be a result of decomposition of side chains and the separation of glycosidic bonds from the xylan structure in switchgrass (Shafizadeh et al., 1972). The weight loss and rate of weight loss of DDGS were significantly different from those of other biomass. Unlike other biomass studied in this project, DDGS is rich in crude protein (30% wt) because it is a byproduct of corn ethanol fermentation. The major weight loss of DDGS was in the temperature range of 200-350 °C. This may be due to the protein and glucan degradation (Wang et al., 2009). In addition, the rate of weight loss of DDGS was much lower as compared to that of switchgrass, wheat straw and eastern redcedar. The rate of weight loss profile for DDGS shows a considerable shift in pattern due to the presence of proteins. This data is also supported from a study by Maddi et al. (2011), which showed that maximum rate of weight loss for proteins occur close to 300 °C.

3.2 Weight loss kinetics of selected biomass materials:

The weight loss kinetic parameters, i.e. activation energy (E), pre exponential factor (A), and order of the reaction (n), for the selected biomass and model components are shown in Table 3. The activation energies for weight loss of cellulose, hemicellulose and lignin were 135.21, 118.54 and 67.62 kJ/mol, respectively. Activation energy and pre-exponential factor for cellulose in this study were consistent with the values reported

by (Jeguirim & Trouvé, 2009; Lewellen et al., 1977; Nada & Hassan, 2000). The kinetic parameters obtained for hemicellulose and lignin decomposition were also consistent with those reported by (Jeguirim & Trouvé, 2009; Murugan et al., 2008; Pasquali & Herrera, 1997; Ramiah, 1970). The variation in activation energies of the model components (cellulose, hemicellulose and lignin) may be attributed to their different chemical structures. Hemicellulose was thermally less stable than cellulose and lignin because of its amorphous nature (Beall & Eickner, 1970). Cellulose required higher activation energy than hemicellulose because of its strong inter-molecular and intra-molecular hydrogen bonding. On the other hand, thermal stability of lignin varied because lignin has a complex structure with many oxygenated functional groups, and the scission of the associated bonds can occur in different temperature ranges (Skreiberg et al., 2011). In the temperature range of 200-400 °C, the scission of weak oxygenated bonds may have required low activation energy.

The temperature range for the weight loss of switchgrass, wheat straw and redcedar were 200-400 °C, while that for the DDGS was 150-500 °C. Switchgrass, wheat straw, eastern redcedar and DDGS decomposed with activation energy of 103.7, 100.67, 90.16 and 31.686 kJ/mol, respectively. Interestingly, although the weight loss kinetic parameters of cellulose, hemicellulose and lignin were found to be different, no significant differences were observed between the weight loss kinetic parameters of the switchgrass, wheat straw and eastern redcedar (Table 3). Only exception was the activation energy of eastern redcedar, which was lower than that of switchgrass and wheat straw possibly because of its high lignin content. Compared to switchgrass, wheat straw and redcedar, much less activation energy was required for DDGS decomposition.

The activation energy and pre exponential factor of DDGS obtained in this study were consistent with values reported by(Wang et al., 2009). Since, reaction kinetics play a vital role in the design optimization of thermochemical units such as pyrolyzers and gasifiers, this information is beneficial from a design perspective, because changing lignocellulosic feedstocks did not show much effect on thermal devolatilization kinetics.

3.3 Gas evolution profiles:

CO_2, CO and CH_4 evolution profiles from switchgrass, wheat straw and eastern redcedar thermal decompositions are shown in the Figs. 4, 5 and 6, respectively. The x-axis shows the temperature of the sample, and y-axis shows the absorbance of gases at the specific wavelengths. Due to the linear relationship between absorbance and gas concentration according to the Beer-Lambert's law, absorbance was used to compare gas evolution profiles in this study. Although the weight loss profiles and kinetic parameters of switchgrass, wheat straw and eastern redcedar were similar, noticeable differences in the concentrations of evolved CO_2, CO and CH_4 were observed. The peaks for maximum concentrations of CO_2, CO and CH_4 were in the temperature range of 500-600 °C. Switchgrass and wheat straw resulted in significantly higher CO, CO_2, but lower CH_4 concentrations as compared to those from eastern redcedar. Generally, cleavage of carbonyl groups from cellulose and hemicellulose degradation results in CO and CO_2 production (Yang et al., 2007). Cellulose may also have produced higher CO due to secondary reactions of primary volatiles and scission of aldehyde groups (R-CHO) (Fu et al., 2010). On the other hand, lignin decomposition has been correlated with methane formation due to cracking of methoxy groups of lignin molecule (Yang et al., 2007; Liu et al., 2008). Thus, as compared to switchgrass and wheat straw, higher lignin content in

eastern redcedar may have resulted in significantly higher methane concentration in the evolved gas.

3.4 Carbon conversion efficiency:

The carbon conversion efficiency is defined as the ratio of carbon available in gaseous and liquid products to the total amount of carbon available in biomass (Lv et al., 2004). The amount of carbon available in tar was not taken into account for calculating the carbon conversion efficiency. Among the biomass model components, cellulose showed the highest conversion efficiency of 99% followed by xylan of 92%. Lignin showed the lowest conversion efficiency of 52%. The conversion efficiencies of model compounds were in good agreement with the values reported by Hanaoka et al. (2005). Among the biomass materials, switchgrass and wheat straw showed highest carbon conversion efficiencies of 94% and 95%, respectively, while both eastern redcedar and DDGS showed a conversion efficiency of 77%. High lignin content in eastern redcedar and high protein content in DDGS may have reduced the carbon conversion efficiency of these substrates significantly.

4. Conclusions:

Weight loss profiles, weigh loss kinetics and gas evolution profiles during thermal decomposition of switchgrass, wheat straw, eastern redcedar and DDGS, and model biomass components were analyzed. Results showed that there was no significant difference in the weight loss profiles of switchgrass, wheat straw and eastern redcedar even though their cellulose, hemicellulose and lignin contents were considerably different. The kinetic parameters such as activation energy, pre-exponential factor

associated with their weight loss were also not significantly different, except for lower activation energy of eastern red cedar. This is an advantage for thermochemical conversion processes considering that similar design of thermochemical reactor units can be needed for many biomass. However, biomass composition significantly influenced the concentrations of evolved CO, CO_2 and CH_4. The CO and CO_2 concentrations from switchgrass and wheat straw were higher than those from eastern red cedar and DDGS because of higher contents of cellulose and hemicellulose in switchgrass and wheat straw. On the other hand, higher lignin content in eastern red cedar resulted in significantly higher CH_4 concentration as compare to switchgrass and wheat straw. In addition, carbon conversion efficiencies for wheat straw (95.0%) and switchgrass (94%) were higher than those for eastern redcedar (77%) and DDGS (77%).

References:

Beall, F.C., Eickner, H.W., 1970. Thermal degradation of wood components: a review of the literature. Forest Products Lab Madison Wis.

Biagini, E., Barontini, F., Tognotti, L., 2006. Devolatilization of Biomass Fuels and Biomass Components Studied by TG/FTIR Technique. *Industrial & Engineering Chemistry Research*, **45**(13), 4486-4493.

Bidlack, J., Malone, M., Benson, R., 1992. Molecular structure and component integration of secondary cell walls in plants. *Proceedings of the Oklahoma Academy of Science.*, **72**, 51-56.

Bridgwater, A.V., 1999. Principles and practice of biomass fast pyrolysis processes for liquids. *Journal of analytical and applied pyrolysis*, **51**(1-2), 3-22.

Bridgwater, T., 2006. Biomass for energy. *Journal of the Science of Food and Agriculture*, **86**(12), 1755-1768.

Carrier, M., Loppinet-Serani, A., Denux, D., Lasnier, J.-M., Ham-Pichavant, F., Cansell, F., Aymonier, C., 2011. Thermogravimetric analysis as a new method to determine the lignocellulosic composition of biomass. *Biomass and Bioenergy*, **35**(1), 298-307.

Chen, W.H., Kuo, P.C., 2010. A study on torrefaction of various biomass materials and its impact on lignocellulosic structure simulated by a thermogravimetry. *Energy*, **35**(6), 2580-2586.

Chouchene, A., Jeguirim, M., Khiari, B., Zagrouba, F., Trouvé, G., 2010. Thermal degradation of olive solid waste: Influence of particle size and oxygen concentration. *Resources, Conservation and Recycling*, **54**(5), 271-277.

Demirbas, A., 2001. Biomass resource facilities and biomass conversion processing for fuels and chemicals. *Energy Conversion and Management*, **42**(11), 1357-1378.

Demirbas, A., 2004. Combustion characteristics of different biomass fuels. *Progress in Energy and Combustion Science*, **30**(2), 219-230.

Evans, R.J., Milne, T.A., 1987. Molecular characterization of the pyrolysis of biomass. *Energy & Fuels*, **1**(2), 123-137.

Fisher, T., Hajaligol, M., Waymack, B., Kellogg, D., 2002. Pyrolysis behavior and kinetics of biomass derived materials. *Journal of analytical and applied pyrolysis*, **62**(2), 331-349.

Fu, P., Hu, S., Xiang, J., Li, P., Huang, D., Jiang, L., Zhang, A., Zhang, J., 2010. FTIR study of pyrolysis products evolving from typical agricultural residues. *Journal of analytical and applied pyrolysis*, **88**(2), 117-123.

Ghetti, P., Ricca, L., Angelini, L., 1996. Thermal analysis of biomass and corresponding pyrolysis products. *Fuel*, **75**(5), 565-573.

Goyal, H., Seal, D., Saxena, R., 2008. Bio-fuels from thermochemical conversion of renewable resources: A review. *Renewable and Sustainable Energy Reviews*, **12**(2), 504-517.

Hames, B., Ruiz, R., Scarlata, C., Sluiter, A., Sluiter, J., Templeton, D., 2008. Preparation of samples for compositional analysis. National Renewable Energy Laboratories. NREL/TP-510-42620.

Hanaoka, T., Inoue, S., Uno, S., Ogi, T., Minowa, T., 2005. Effect of woody biomass components on air-steam gasification. *Biomass and Bioenergy*, **28**(1), 69-76.

Hill, J., Nelson, E., Tilman, D., Polasky, S., Tiffany, D., 2006. Environmental, economic, and energetic costs and benefits of biodiesel and ethanol biofuels. *Proceedings of the National Academy of Sciences*, **103**(30), 11206.

Jefferson, P.G., McCaughey, W.P., May, K., Woosaree, J., McFarlane, L., 2004. Potential utilization of native prairie grasses from western Canada as ethanol feedstock. *Canadian journal of plant science*, **84**(4), 1067-1075.

Jeguirim, M., Trouvé, G., 2009. Pyrolysis characteristics and kinetics of Arundo donax using thermogravimetric analysis. *Bioresource Technology*, **100**(17), 4026-4031.

Johnson, D., Adam, P., Ashley, P., Chum, H., Deutch, S., Fennel, J., Wiselogel, A., 1994. Study of compositional changes in biomass feedstocks upon storage (results). *Rapport-Sveriges Lantbruksuniversitet, Institutionen foer Virkeslaera*.

Kumar, A., Eskridge, K., Jones, D.D., Hanna, M.A., 2009. Steam-air fluidized bed gasification of distillers grains: Effects of steam to biomass ratio, equivalence ratio and gasification temperature. *Bioresource Technology*, **100**(6), 2062-2068.

Kumar, A., Wang, L., Dzenis, Y.A., Jones, D.D., Hanna, M.A., 2008. Thermogravimetric characterization of corn stover as gasification and pyrolysis feedstock. *Biomass and Bioenergy*, **32**(5), 460-467.

Lettner, F., Timmerer, H., Haselbacher, P., 2007. Biomass gasification–State of the art description. *Graz Univ. Tech.-Institute of thermal engineering*.

Lewellen, P., Peters, W., Howard, J., 1977. Cellulose pyrolysis kinetics and char formation mechanism. Elsevier. pp. 1471-1480.

Liu, Q., Wang, S., Zheng, Y., Luo, Z., Cen, K. 2008. Mechanism study of wood lignin pyrolysis by using TG–FTIR analysis. *Journal of analytical and applied pyrolysis*, **82**(1), 170-177.

Lv, P., Xiong, Z., Chang, J., Wu, C., Chen, Y., Zhu, J., 2004. An experimental study on biomass air-steam gasification in a fluidized bed. *Bioresource Technology*, **95**(1), 95-101.

Maddi, B., Viamajala, S., Varanasi, S., 2011. Comparative study of pyrolysis of algal biomass from natural lake blooms with lignocellulosic biomass. *Bioresource Technology*, **102**(23), 11018-11026.

Mani, T., Murugan, P., Abedi, J., Mahinpey, N., 2010. Pyrolysis of wheat straw in a thermogravimetric analyzer: Effect of particle size and heating rate on devolatilization and estimation of global kinetics. *Chemical Engineering Research and Design*, **88**(8), 952-958.

Mansaray, K.G., Ghaly, A.E. 1999. Determination of Reaction Kinetics of Rice Husks in Air Using Thermogravimetric Analysis. *Energy Sources, Part A: Recovery, Utilization, and Environmental Effects*, **21**(10), 899 - 911.

McGinnis, G.D., Shafizadeh, F., 1980. Cellulose and hemicellulose. in: *Pulp and Paper: Chemistry and Chemical Technology*, (Ed.) J.P. Casey, John Wiley and Sons. New York, pp. 1-31.

Meier, D., Faix, O., 1999. State of the art of applied fast pyrolysis of lignocellulosic materials-a review. *Bioresource Technology*, **68**(1), 71-77.

Mohan, D., Pittman, C.U., Jr., Steele, P.H., 2006. Pyrolysis of wood/biomass for bio-oil: A critical review. *Energy & Fuels*, **20**(3), 848-889.

Mulkey, V., Lee, V., 2006. Management of switchgrass-dominated conservation reserve program lands for biomass production in South Dakota. *Crop Science*, **46**(2), 712.

Murugan, P., Mahinpey, N., Johnson, K.E., Wilson, M., 2008. Kinetics of the pyrolysis of lignin using thermogravimetric and differential scanning calorimetry methods. *Energy & Fuels*, **22**(4), 2720-2724.

Nada, A., Hassan, M.L., 2000. Thermal behavior of cellulose and some cellulose derivatives. *Polymer degradation and stability*, **67**(1), 111-115.

Ounas, A., Aboulkas, A., El harfi, K., Bacaoui, A., Yaacoubi, A., 2011. Pyrolysis of olive residue and sugar cane bagasse: Non-isothermal thermogravimetric kinetic analysis. *Bioresource Technology*, **102**(24), 11234-11238.

Pasquali, C., Herrera, H., 1997. Pyrolysis of lignin and IR analysis of residues. *Thermochimica acta*, **293**(1-2), 39-46.

Pérez, J., Munoz-Dorado, J., De la Rubia, T., Martinez, J. 2002. Biodegradation and biological treatments of cellulose, hemicellulose and lignin: an overview. *International Microbiology*, **5**(2), 53-63.

Ramiah, M., 1970. Thermogravimetric and differential thermal analysis of cellulose, hemicellulose, and lignin. *Journal of Applied Polymer Science*, **14**(5), 1323-1337.

Raveendran, K., Ganesh, A., Khilar, K.C., 1996. Pyrolysis characteristics of biomass and biomass components. *Fuel*, **75**(8), 987-998.

Ryu, C., Yang, Y.B., Khor, A., Yates, N.E., Sharifi, V.N., Swithenbank, J., 2006. Effect of fuel properties on biomass combustion: Part I. Experiments—fuel type, equivalence ratio and particle size. *Fuel*, **85**(7-8), 1039-1046.

Shafizadeh, F., McGinnis, G.D., Philpot, C.W., 1972. Thermal degradation of xylan and related model compounds. *Carbohydrate Research*, **25**(1), 23-33.

Skreiberg, A., Skreiberg, Ø., Sandquist, J., Sørum, L., 2011. TGA and macro-TGA characterisation of biomass fuels and fuel mixtures. *Fuel*, **90**(6), 2182-2197.

Sluiter, A., Hames, B., Ruiz, R., Scarlata, C., Sluiter, J., Templeton, D., 2008. Determination of ash in bimoass. National Renewable Energy Laboratories. NREL/TP-510-42622.

Sluiter, A., Hames, B., Ruiz, R., Scarlata, C., Sluiter, J., Templeton, D., Crocker, D., 2008b. Determination of Structural Carbohydrates and Lignin in Biomass. (April 2008). National Renewable Energy Laboratory.NREL/TP-510-42618.

Sluiter, A., Ruiz, R., Scarlata, C., Sluiter, J., D. Templeton, 2008a. Determination of Extractives in Biomass. National Renewable Energy Laboratory. NREL/TP-510-42619.

Tilman, D., Hill, J., Lehman, C., 2006. Carbon-negative biofuels from low-input high-diversity grassland biomass. *Science*, **314**(5805), 1598.

Wang, L., Kumar, A., Hanna, M., Weller, C.L., Jones, D., 2009. Thermal Degradation Kinetics of Distillers Grains and Solubles in Nitrogen and Air. *Energy Sources, Part A*, **31**(10), 797-806.

Williams, P.T., Besler, S., 1993. The pyrolysis of rice husks in a thermogravimetric analyser and static batch reactor. *Fuel*, **72**(2), 151-159.

Xie, W., Pan, W.P., 2001. Thermal characterization of materials using evolved gas analysis. *Journal of thermal analysis and calorimetry*, **65**(3), 669-685.

Yaman, S., 2004. Pyrolysis of biomass to produce fuels and chemical feedstocks. *Energy Conversion and Management*, **45**(5), 651-671.

Yang, H., Yan, R., Chen, H., Lee, D.H., Zheng, C., 2007. Characteristics of hemicellulose, cellulose and lignin pyrolysis. *Fuel*, **86**(12–13), 1781-1788.

Zabaniotou, A., Ioannidou, O., Antonakou, E., Lappas, A., 2008. Experimental study of pyrolysis for potential energy, hydrogen and carbon material production from lignocellulosic biomass. *International Journal of Hydrogen Energy*, **33**(10), 2433-2444.

Figures:

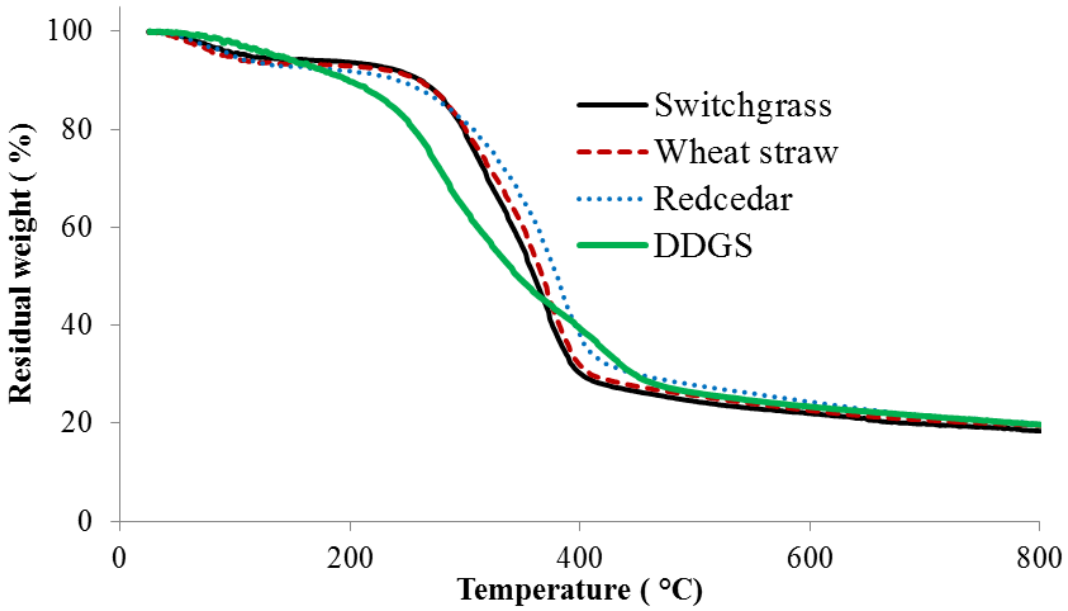

Figure.1. Weight loss profiles of switchgrass, wheat straw, eastern redcedar and DDGS. Each trend is an average of two replicates. Statistical analysis showed no difference between the weight loss profiles for the four different biomass types.

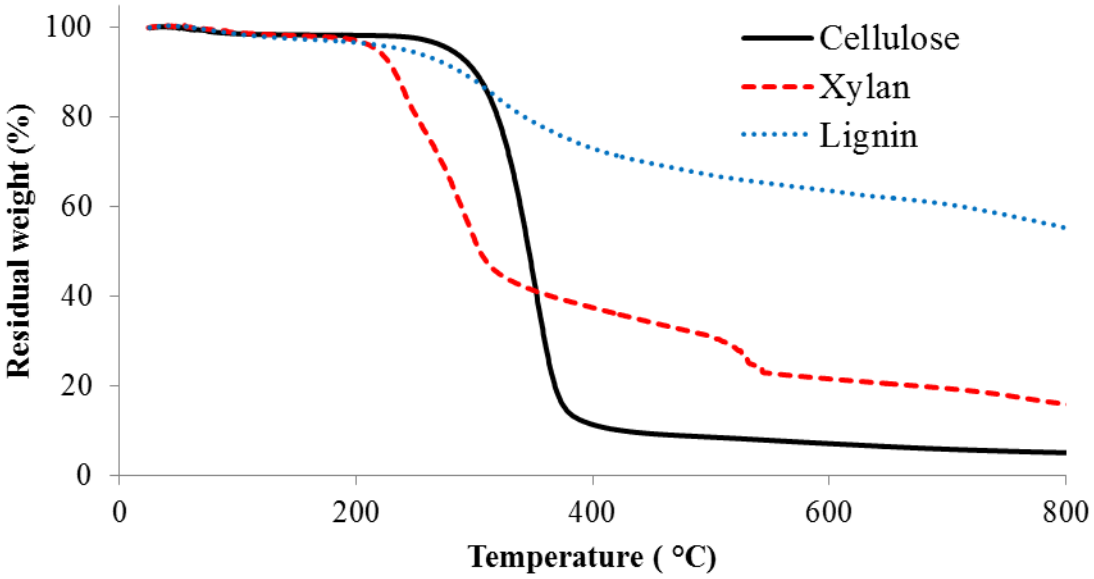

Figure.2. Weight loss profiles of Cellulose, xylan and lignin. Each trend is an average of two replicates. Statistical analysis showed significant difference between the weight loss profiles of the three biomass model compounds.

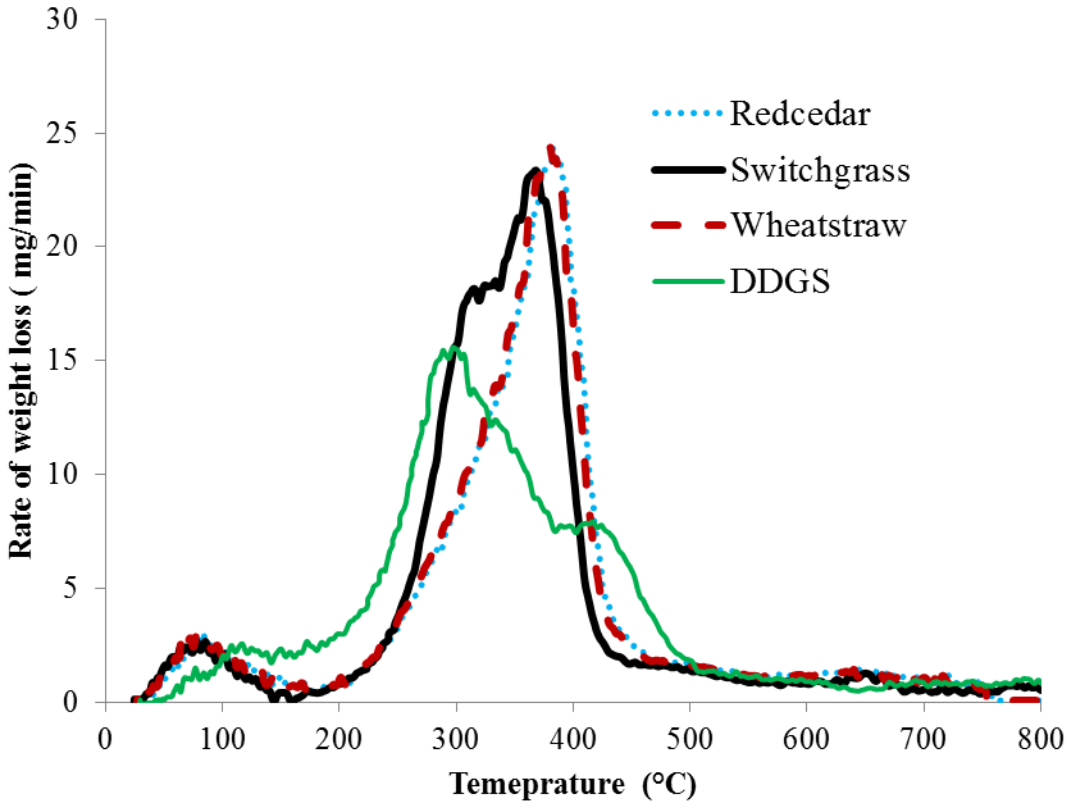

Figure.3. Rate of weight loss profiles of switchgrass, wheat straw, eastern red cedar and DDGS. Each trend is an average of two replicates.

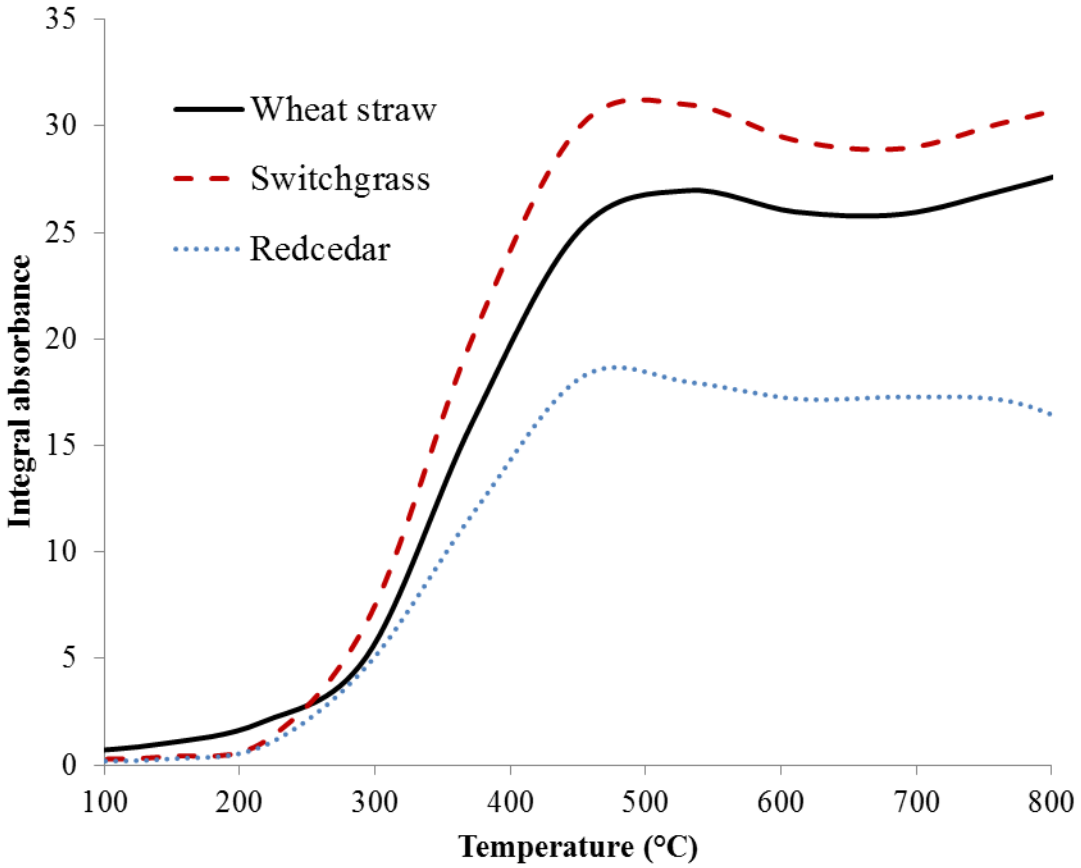

Figure.4. Evolved CO_2 as a function of temperature during switchgrass, wheat straw and eastern redcedar decomposition. Each trend is an average of two replicates. Effect of biomass type on CO_2 concentration was significant (p=0.0003). Fisher's LSD test on maximum concentrations of CO2 released from different biomass showed significant differences between them, at 95% confidence interval.

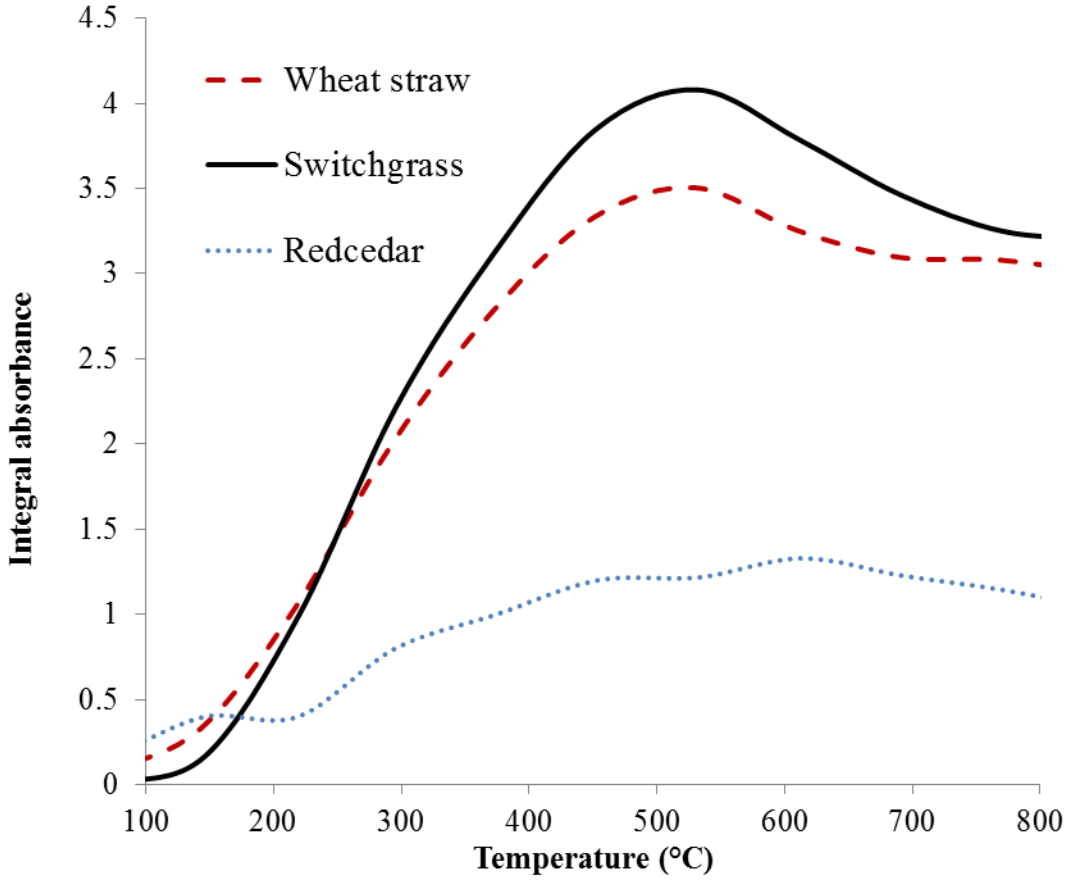

Figure.5. Evolved CO as a function of temperature during switchgrass, wheat straw and eastern redcedar decomposition. Each trend is an average of two replicates. Effect of biomass type on CO concentration was significant ($p<0.0001$). Fisher's LSD test on maximum concentrations of CO released from different biomass showed significant differences between them, at 95% confidence interval.

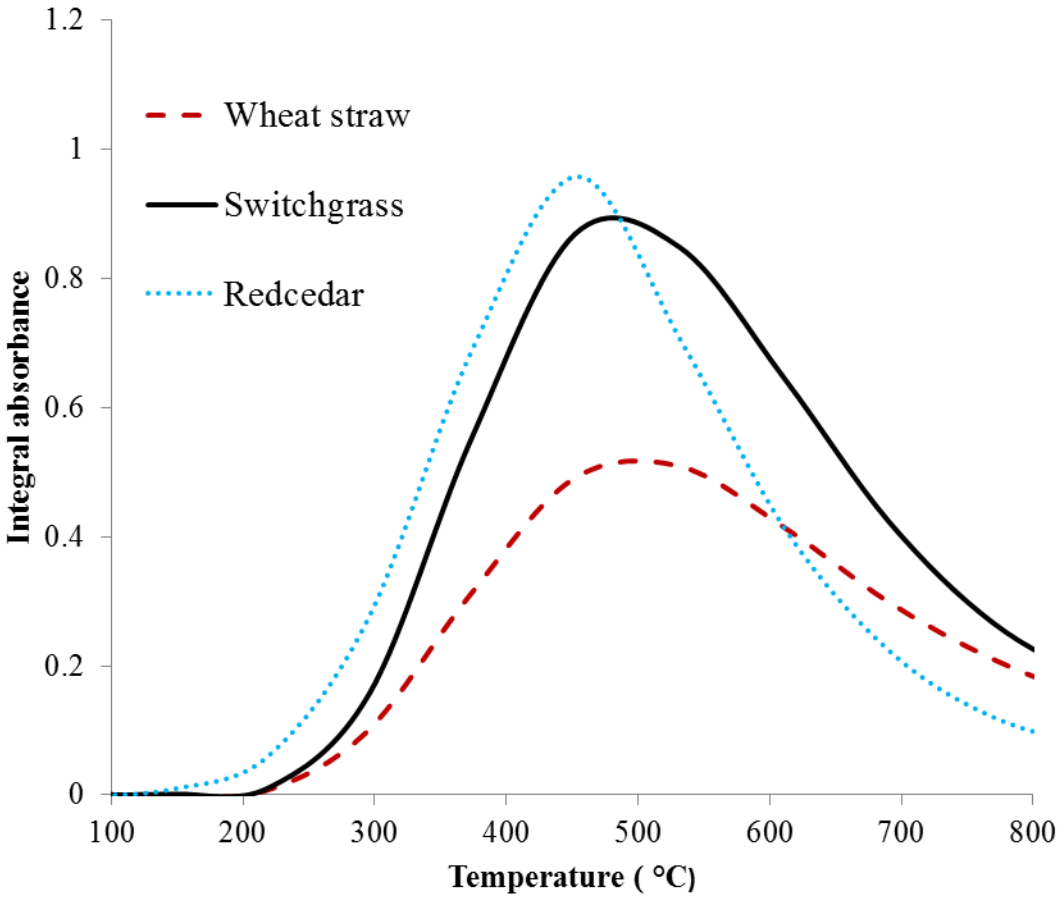

Figure.6. Evolved CH_4 as a function of temperature during switchgrass, wheat straw and redcedar decomposition. Each trend is an average of two replicates. Effect of biomass type on CH_4 concentration was significant (p=0.0003). Fisher's LSD test showed that maximum CH_4 concentration of released from eastern red cedar was significant higher than that from wheat straw and switchgrass, at 95% confidence interval.

Table 1. Ultimate analysis (% wt. on dry basis) of the selected biomass and components

Elements	Switchgrass	Wheat straw	Eastern redcedar	DDGS	Cellulose	Xylan	Lignin
Carbon	46.62	43.2	51.07	49	42.96	43.25	57.7
Hydrogen	5.74	5.0	5.97	6.3	6.3	6.2	4.38
Oxygen	42.27	39.4	40.95	33.6	50.74	49.9	34
Nitrogen	0.18	0.61	0.37	4.5	0.0	0.0	0.11
Sulphur	0.3	0.11	0.0	0.4	0.0	0.0	3.22

Table.2. Chemical composition of switchgrass, wheat straw, eastern redcedar and DDGS

Composition (%dry)	Switchgrass	Wheat straw	Eastern Redcedar	DDGS (Kim et al., 2008)
Glucan	38.46 ± 0.69^{B}	$39.18 \pm 2.01^{A,B}$	40.30 ± 1.50^{A}	16.00 ± 0.10^{C}
Xylan	26.34 ± 0.54^{A}	24.62 ± 1.36^{B}	8.50 ± 0.04^{C}	8.20 ± 0.07^{C}
Galactan	1.16 ± 0.18^{B}	$0 \pm 0^{B,C}$	2.00 ± 0.60^{A}	0 ± 0^{C}
Arabinan	3.41 ± 0.32^{B}	1.68 ± 0.25^{C}	1.40 ± 1.00^{C}	5.30 ± 0.02^{A}
Mannan	0.13 ± 0.22^{B}	0 ± 0^{C}	6.00 ± 1.20^{A}	0 ± 0^{B}
Lignin	21.40 ± 0.24^{B}	17.17 ± 0.46^{C}	35.90 ± 0.70^{A}	0 ± 0^{D}
Ash	1.91 ± 0.10^{B}	2.12 ± 0.87^{B}	0.30 ± 0.00^{C}	4.50 ± 0.07^{A}

Values listed are average of 6 replicates ± standard deviation. Values in the same row and with the same letter are not statistically different at 95% confidence interval.

Table 3. Weight-loss kinetic parameters of the selected biomass and model components

Sample	T (°C)	E (kJ mol^{-1})	A × 10^5 (S^{-1})	n	R^2
Switchgrass	200-390	103.70^{C}	1063^{B}	0.67^{B}	0.99
Wheat straw	200-390	100.67^{C}	1915^{B}	0.68^{B}	0.99
Eastern red cedar	200-400	90.16^{D}	1775^{B}	0.68^{B}	0.98
DDGS	150-500	31.67^{F}	0.0049^{D}	0.45^{D}	0.92
Cellulose	250-360	135.21^{A}	3020000^{A}	0.77^{A}	0.97
Xylan	200-280	118.54^{B}	3025000^{A}	$0.47^{C,D}$	0.97
Lignin	200-340	67.62^{E}	4.04^{C}	0.50^{C}	0.96

Values listed are average of two replicates. Values in the same column with the same letter are not statistically significant at 95% confidence interval. A log transformation of data was performed on the values of A prior to performing post-hoc statistical analysis using Fisher's LSD test.

CHAPTER IV

Numerical simulation of switchgrass gasification using finite rate chemistry

Abstract:

Fluidized bed gasification is a process involving complex multiphase reactions coupled with heat and mass transfer. Computational Fluid Dynamics CFD modeling provides a better understanding of complex processes and aids in process optimization and scale up. The goal of this study was to develop a three dimensional CFD model capable of describing the switchgrass gasification process in a fluidized bed reactor. The model was developed using commercial software ANSYS FLUENT 13.0**.** Euler-Lagrangian multiphase approach was used to model gas and solid phases. The model was able to simulate detailed chemistry of gasification by taking drying, devolatilization and chemical reactions such as homogeneous and heterogeneous reactions into account. Unlike other CFD gasification models, the kinetic parameters required for devolatilization were derived from thermogravimetric analysis of switchgrass in nitrogen atmosphere. The reaction rates for homogeneous and heterogeneous reactions were described using the finite rate/eddy dissipation model.

The simulation results provided detailed information on temperature and species concentration profiles inside the reactor. The non-uniform distribution of temperature in the reactor showed the different reaction zones for devolatilization, combustion and gasification. Regarding species concentrations, higher CO_2 was observed in the combustion zone; whereas, concentrations of CO, H_2 and CH_4 were higher in the gasification zone. The model validation was performed by comparing the predicted outlet concentrations of the gases with experimental data. The sensitivity of the model was also analyzed by carrying the simulations for two ER values of 0.32 and 0.29.

Keywords: CFD, Euler-Lagrangian, devolatilization, turbulence, biomass gasification.

1. Introduction:

Fluidized bed reactors are widely in use for thermochemical conversion processes such as combustion, gasification and pyrolysis. Excellent solid gas mixing, proper temperature distribution and high heat and mass transfer within the reactors are the major advantages associated with fluidized beds (Schmidt & Renz, 2000; Yu et al., 2007). Even though gasification technology has been around for many centuries, knowledge on the detailed hydrodynamics and complex chemical reactions in fluidized bed gasifiers is still lacking (Lavoie et al.). Moreover, the experimental determination of heat and mass transfer within the reactor is complicated and expensive. A good understanding of underlying physical and chemical phenomenon of thermal decomposition of materials is critical for optimization and scale up purposes (Didwania A & Robert, 2009). In this regard, Computational Fluid Dynamics (CFD) modeling appears to be a relatively inexpensive and promising tool to simulate solid fluid flows and chemical reactions (Sundaresan, 2000). The extent to which CFD can be used for simulation purposes is limited based on the computation power available. In recent years, increased computational power and capabilities allow CFD simulations to be done at a relatively faster pace (Kutler, 1989; Westbrook et al., 2005). To date, most computational research was conducted on coal gasification and combustion processes in fixed and fluidized bed reactors. A three dimensional model was developed to simulate a coal gasification process in a pressurized spout fluidized bed to predict gas composition (Deng et al., 2008). A CFD study on coal gasification in a bubbling fluidized bed was carried out to understand the effects of bed temperature, bed material and height (Armstrong et al., 2011). The authors concluded that the composition of the exiting gas

emissions was strongly influenced by the bed composition, variation in the bed height and the temperature of the bed.

In recent years, biomass gasification is emerging due to the renewable nature of biomass. Even though biomass and coal can be distinguished in terms of physical and chemical properties, the governing equations that describe their gasification process are not very different. The reactivity of biomass is higher than coal and devolatilizes at a faster rate. Thus, the reaction rates for coal gasification may not be directly applicable to biomass. However, with some caution, the elements of governing equations that describe coal gasification are applicable to biomass as well (Gómez-Barea & Leckner, 2010).

Among the available CFD modeling techniques, discrete phase modeling (DPM) and multiphase or two phase modeling (TPM) are quite successful in simulating the gasification process in fluidized bed reactors (Oevermann et al., 2009). However, taking computational power into account, most of the computational research was done based on two phase modeling (Gera et al., 1998; Ibsen et al., 2004). This modeling follows the eulerian-eulerian approach, which assumes gas and solid phases as continuous and interpenetrating (Kuipers et al., 1992; Patil et al., 2006; Schmidt & Renz, 2000) . On the other hand, DPM follows eulerian-lagrangian approach, which tracks each particle and simulates its dynamics. Even though the computational power requirements of discrete phase modeling are higher than that of multiphase flow modeling, the detailed dynamics of particle motion is possible by taking particle-particle and particle wall collisions into account (Ibsen et al., 2004; Oevermann et al., 2009).

Most of the models used for CFD gasification were two dimensional models (Busciglio et al., 2009; Gerun et al., 2008; Marklund et al., 2007; Rogel & Aguillón, 2006). Since these models do not fully account for local effects, the predictions might not be sufficient for scale up studies. In addition, the kinetic parameters such as activation energy and pre exponential factor required for devolatalization were adopted from literature. The novelty of the present study was use of kinetic parameters obtained from thermogravimetric analysis of switchgrass in inert atmosphere and development of a CFD model for gasification. Moreover, no studies have been conducted on switchgrass gasification modeling using CFD. The specific objectives were to 1) numerically investigate the distribution of temperature and gas species such as CO, CO_2, H_2, CH_4, and C_2H_4 inside the fluidized bed gasifier and 2) validate the numerical model by comparing the outlet gas concentrations and temperature predictions with experimental data.

2. Numerical modeling procedure:

2.1 Governing equations:

In CFD, the continuous phase computations are represented by a basic set of equations such as mass, momentum, energy and species transport conservation equations.

The mass conservation equation for gas phase is,

$$\frac{\partial}{\partial t}(\rho) + \nabla \cdot (\rho V_g) = s_g \quad (1)$$

The momentum conservation equation for gas phase is,

$$\frac{\partial}{\partial t}(\rho\vec{v}) + \nabla \cdot (\rho\vec{v}\vec{v}) = -\nabla p + \nabla \cdot (\bar{\bar{\tau}}) + \rho\vec{g} + \vec{F} \quad (2)$$

The energy conservation equation for gas phase is,

$$\frac{\partial}{\partial t}(\rho E) + \nabla \cdot \left(\vec{v} \cdot (\rho E + p)\right) = \nabla \cdot \left(\left(k_{eff}\nabla T\right) - \sum_j h_j J_j + \left(\bar{\bar{\tau}}_{eff} \cdot \vec{v}\right)\right) + S_h \quad \ldots (3)$$

The species conservation equations is,

$$\frac{\partial(\rho Y_i)}{\partial t} + \nabla \cdot (\rho\vec{u}\, Y_i) = \nabla \cdot \left(D\nabla(\rho Y)\right) + S_Y + R_f \quad \ldots (4)$$

where,

Sm, Su and S_H are the source terms added to continuous phase from the particles in discrete phase. R_f is the source term due to chemical reactions.

2.2 Realizable k-ε turbulent model:

To simulate the turbulence dynamics during gasification, realizable k-ε model was used. To account for velocity fluctuations due to turbulence in the flow field, eddy viscosity (not a property of fluid) was calculated. Different methods are available to calculate eddy viscosity based on the number of equations solved. In this study, a realizable k-ε turbulent model was chosen that solves transport equations for turbulent kinetic energy (k) and turbulent dissipation rate (ε) to calculate eddy viscosity.

The transport equation for turbulent kinetic energy is,

$$\frac{\partial(\rho k)}{\partial t} + \nabla \cdot (\rho\vec{u}\, k) - \nabla \cdot \left(\left(\mu + \frac{\mu_T}{\sigma_k}\right) \cdot \nabla k\right) = G_k + G_b - \rho\varepsilon \quad .. (5)$$

The transport equation for turbulent dissipation rate is,

$$\frac{\partial(\rho\varepsilon)}{\partial t} + \nabla \cdot (\rho\vec{u}\,\varepsilon) - \nabla \cdot \left(\left(\mu + \frac{\mu_T}{\sigma_\varepsilon} \right) \cdot \nabla\varepsilon \right) = c_{1\varepsilon} \cdot \frac{\varepsilon}{k}(G_k + c_{3\varepsilon}G_b) - c_{2\varepsilon}\frac{\rho\varepsilon^2}{k} \quad \text{.. (6)}$$

The turbulent eddy viscosity is calculated by,

$$\mu_T = \rho C_\mu \frac{k^2}{\varepsilon} \quad \text{… (7)}$$

2.3 Chemical reactions:

Biomass gasification process consists of dying, devolatilization, char oxidation and reduction.

2.3.1 Drying:

Drying was modeled using a wet combustion model. In this model, the moisture in the biomass evaporates when it reaches the boiling point (Guide, 2011). The volume fraction of water was an input to the model, which was calculated based on the mass fraction of moisture content specified in the proximate analysis of switchgrass (Table 2).

2.3.2 Devolatalization:

Devolatilization is primary pyrolysis which describes the decomposition of solid biomass into gases, tar and solid char in inert atmosphere. In this model, it was assumed that all the tar was converted into gaseous species. The devolatilization reaction can be written as follows (Gómez-Barea & Leckner, 2010; Kumar et al., 2009b) :

$$\text{Biomass} \xrightarrow{k} \text{Volatiles} + \text{char} + \text{water} \quad \text{.. (8)}$$

$$\text{Volatiles} \xrightarrow{k} \text{aCO} + \text{b}CH_4 + \text{cH}_2 + \text{d } H_2S + \text{e } NH_3 + \text{f } C_2H_4 + g\ H_2O \quad \text{.. (9)}$$

The reaction kinetic parameters such as activation energy (E) and pre exponential factor (A) for the devolatilization equation were obtained from our thermogravimetric experiments on switchgrass in a nitrogen atmosphere (Table 1).

2.3.3 Gas phase and char reactions:

The homogenous gas phase reactions are described as follows:

Water gas shift reaction: $CO + H_2O \leftrightarrow CO_2 + H_2$ ... (10)

CO partial combustion: $CO + 1/2\ O_2 \rightarrow 2CO_2$ … (11)

H_2 partial combustion: $H_2 + 1/2O_2 \rightarrow H_2O$ ..... (12)

CH_4 combustion: $CH_4 + 2O_2 \rightarrow CO_2 + 2\ H_2O$ …..(13)

The rate expressions and kinetic parameters for the above reactions were taken from (Fletcher et al., 2000) and are shown in Table 1.

The heterogeneous reactions described as follows:

Char combustion: $C<s> + O_2 \rightarrow CO_2$ (14)

Boudouard reaction: $C<s> + CO_2 \rightarrow 2CO$ (15)

Water gas reaction: $C<s> + H_2O \rightarrow CO + H_2$ (16)

Methanation reaction: $C<s> + 2H_2 \rightarrow CH_4$ (17)

The reaction kinetic parameters for char oxidation were obtained from (Fletcher et al., 2000) and are shown in Table 1.

2.4 Computational set up:

A three dimensional computational set up was developed as shown in Fig. 1. A quadrilateral sweep mesh with 14,874 elements and 17,145 nodes was employed as a numerical grid. Since quadrilateral mesh provides higher accurate solution with fewer cells for simple geometries such as fluidized beds, it was chosen over triangular mesh. The smallest face size of computational grid was 0.0009 m and the largest size was 0.00134 m. Finite volume discretization scheme was employed, which solves a set of algebraic equations instead of partial differential equations for each volume. Second order discretization was employed for better accuracy with a time step size of 1×10^{-4}.

2.4.1 Initial and boundary conditions:

At air and fuel inlets, mass flow rates were prescribed as boundary conditions. At an outlet boundary condition, the pressure was fixed as atmospheric. No slip boundary condition was prescribed at the walls for velocity. The bed was initially packed with sand material with the total volume fraction of solids equal to 0.60. An initial temperature of 673K was patched to the solid to start the gasification process. The material properties from proximate and ultimate analyses were inputs to the model (Table 2). The experimental data used in this study was obtained using a lab scale bubbling fluidized bed at Oklahoma State University.

A small time step of 1×10^{-4} s was used due to the different time scales of the hydrodynamics and different scales of reaction rates. Initially, the simulation was carried out without considering heat transfer and gasification reactions. Once the solution to the

hydrodynamics reached steady state, the simulations were carried out by enabling heat transfer and gasification reactions.

2.4.2 Model assumptions:

The following assumptions were made in the model.

1. Axis of symmetry was assumed when modeling the reactor to reduce computational power.
2. Switchgrass, char and sand particles were assumed to be in spherical shape.
3. The char particles were treated as 100% carbon. Ash was taken into consideration separately.

3 Results and Discussion:

3.1 Temperature distribution:

The asymmetric distribution of temperature can be seen in Fig. 2. The existence of non-uniformity in the temperature profiles was due to the various reactions (endothermic and exothermic) occurring at different locations within the gasifier. The average axial temperature distribution is illustrated in Fig. 3. The gasification process region can be divided into three zones, which are pyrolysis, combustion and gasification. The pyrolysis, combustion and gasification zones were in the range of 0.0 -0.124 m, 0.124 - 0.254 m and 0.254- 1.295 m, respectively. In the pyrolysis zone, drying and devolatilization reactions were dominant. Drying of biomass releases moisture and devolatilization breaks down the biomass into various gaseous species, ash and char. Thus, the nature of these reactions is endothermic. Hence, they resulted in low

temperature in the pyrolysis zone as shown in Figure 3. After devolatalization, the evolved gaseous species and char reacted with oxygen in the combustion zone due to the high availability of oxygen. In the combustion zone, the partial combustion reactions were dominant and resulted in increase in the temperature. The maximum average temperature predicted in this zone was 1,034 K. The presence of a sand bed in this zone also enhanced the reactions and contributed to the increase in temperature. However, a high temperature of 1,600 K was noticed in some locations within the combustion zone. Complete combustion might have resulted in these hot spots. In the gasification zone, the availability of oxygen was low; hence, the partial combustion reactions were less prominent. The endothermic reactions such as the Boudouard (eq.15) and water gas (eq. 16) reactions played a major role leading to the decrease in temperature. A uniform temperature distribution was observed in the radial direction due to proper mixing. The simulated temperature profiles in the axial dimension were in fairly good agreement with experimental data as shown in Figure 3.

3.2 Gas composition distribution:

The distributions of product gases such as CO_2, CO, H_2, CH_4, C_2H_4, N_2 and O_2 in the gasifier are illustrated in Figures 4 and 5. The concentration of CO_2 was not uniform along the height of the gasifier as shown in Figure 4(a). High concentration of CO_2 was observed in the combustion zone because of the partial combustion of char (eq. 14) and CO (eq.11). On the other hand, opposite trends were noticed for CO and H_2 concentration distributions as illustrated in figures 4(c) and (d). Boudouard (eq.15), water gas (eq.16) and water gas shift (eq.10) reactions played major roles in the gasification zone. These reactions resulted in high concentrations of CO and H_2 in this

zone. CH_4 was asymmetrically distributed along the height of the reactor as shown in Fig. 4(b). CH_4 produced from devolatilization was partly consumed in combustion reactions. Hence, CH_4 concentration was low in the combustion zone. However, in the gasification zone, CH_4 concentration increased due to the methane reforming (eq.17) reaction. In the combustion zone, oxygen was completely consumed in partial combustion reactions of CO, CH_4 and char. Thus, the concentration of oxygen was sharply decreased to zero as it entered the combustion zone (Fig. 5(f) and 7). The concentration of N_2 decreased in the pyrolysis and combustion zone due to the evolution of gaseous species that diluted the N_2 concentration. In the gasification zone, the gaseous species further reacted and affected the composition of other gaseous species as described above. However, the concentration of N_2 remained same. The concentrations of all the gaseous species remained constant in the free board zone (Fig. 6 and 7).

3.3 Model validation and sensitivity analysis:

The model was validated by comparing the simulated results of product gas concentrations at the outlet with experimental data for two values of equivalence ratio (ER) i.e., 0.32 and 0.29. The comparison is illustrated in Fig. 8. In the case of ER = 0.32, the error between predicted and experimental values of CO, CO_2, N_2 and CH_4 concentrations were less than 10%. The error in the prediction of H_2 concentration was less than 15%. In the case of ER= 0.29, the error in concentration of all gas species excluding CH_4 was less than 5%. The error in CH_4 concentration was 25%, which is the highest compared to those of other gas species. Since the concentration of CH_4 was low in both experimental and numerical results, a small difference resulted in a high error value. For validation, predicted temperature at the outlet was also compared with the

experimental data and the error was less than 10 %. Overall, the model was able to predict yields of biomass gasification process with reasonable accuracy. The concentration profiles of the gaseous species for the two ER values are shown in Fig. 8(a) and 8 (b). From the figures, it can be observed that with slight variation in the ER, the predicted concentration of the gaseous species varied considerably indicating that the model was sensitive to small changes in the ER.

4. Conclusions:

A three dimensional CFD model was developed to simulate fluidized bed gasification using the Euler-Lagrangian multiphase approach. The detailed chemistry of gasification was modeled by employing kinetics for devolatilization, homogeneous and heterogeneous reactions. From the predicted results, non-uniform temperature distribution was observed along the height of the gasifier. The temperature was high in the bed region due to the dominance of exothermic oxidation reactions. Low temperature was observed in gasification zone due to the dominance of endothermic reactions. The predicted temperature was in good agreement with experimental data with a calculation error of less than 10 %. Product gas species concentration profiles were asymmetrically distributed inside the reactor. CO_2 concentration was the highest in combustion zone due to the partial combustion reactions of CO and char. High concentrations of CO and H_2 were predicted in gasification zone due to the dominance of water shift and boudouard reactions. Methanation reaction resulted in higher CH_4 concentration in gasification zone. The predicted concentrations of the species at the outlet were compared against the experimental data at two ERs of 0.32 and 0.29. There

was a good agreement between numerical and experimental results with overall error of less than 15%.

Nomenclature:

$\vec{F}$ - external body forces (N)

G_k-generation of turbulent kinetic energy due to mean velocity gradients

G_b-generation of turbulent kinetic energy due to buoyancy

h_j- sensible enthalpy of species j (J/kg)

J_j -diffusion flux of species j (kg/m^2s)

k_{eff} -effective conductivity

k- turbulent kinetic energy

p-static pressure

R_f-source term due to chemical reactions

S_h-heat of chemical reaction

S_m- mass added to the continuous phase from dispersed phase

$\vec{v}$ -velocity vector (m/s)

Y_i-mass fraction

Greek symbols:

ρ- density of gas (kg/m^3)

$\bar{\bar{\tau}}$ -stress tensor (Pa)

ε-turbulent dissipation rate (w/m^3)

References:

A. Sluiter, B.H., R. Ruiz, C. Scarlata, J. Sluiter, D. Templeton, and D. Crocker. 2008a. Determination of Extractives in Biomass. (April 2008).

A. Sluiter, B.H., R. Ruiz, C. Scarlata, J. Sluiter, D. Templeton, and D. Crocker. 2008b. Determination of Structural Carbohydrates and Lignin in Biomass. (April 2008).

Al-Harahsheh, M., Al-Ayed, O., Robinson, J., Kingman, S., Al-Harahsheh, A., Tarawneh, K., Saeid, A., Barranco, R. 2011. Effect of demineralization and heating rate on the pyrolysis kinetics of Jordanian oil shales. *Fuel Processing Technology*, **92**(9), 1805-1811.

Armstrong, L.M., Gu, S., Luo, K.H. 2011. Parametric Study of Gasification Processes in a BFB Coal Gasifier. *Industrial & Engineering Chemistry Research*, **50**(10), 5959-5974.

Beall, F.C., Eickner, H.W. 1970. Thermal degradation of wood components: a review of the literature.

Biagini, E., Barontini, F., Tognotti, L. 2006. Devolatilization of Biomass fuels and Biomass components studied by TG/FTIR technique. *Industrial & Engineering Chemistry Research*, **45**(13), 4486-4493.

Biagini, E., Guerrini, L., Nicolella, C. 2009. Development of a Variable Activation Energy Model for Biomass Devolatilization. *Energy & Fuels*, **23**(6), 3300-3306.

Biagini, E., Tognotti, L. TG-FTIR analysis of biomass and biomass components during devolatilisation.

Bidlack, J., Malone, M., Benson, R. 1992. Molecular structure and component integration of secondary cell walls in plants. *Proceedings of the Oklahoma Academy of Science.*, **72**, 51-56.

Branca, C., Albano, A., Di Blasi, C. 2005. Critical evaluation of global mechanisms of wood devolatilization. *Thermochimica Acta*, **429**(2), 133-141.

Bridgwater, A. 1999. Principles and practice of biomass fast pyrolysis processes for liquids. *Journal of analytical and applied pyrolysis*, **51**(1-2), 3-22.

Bridgwater, T. 2006. Biomass for energy. *Journal of the Science of Food and Agriculture*, **86**(12), 1755-1768.

Busciglio, A., Vella, G., Micale, G., Rizzuti, L. 2009. Analysis of the bubbling behaviour of 2D gas solid fluidized beds:: Part II. Comparison between experiments and numerical simulations via Digital Image Analysis Technique. *Chemical Engineering Journal*, **148**(1), 145-163.

Carrier, M., Loppinet-Serani, A., Denux, D., Lasnier, J.-M., Ham-Pichavant, F., Cansell, F., Aymonier, C. 2011. Thermogravimetric analysis as a new method to determine the lignocellulosic composition of biomass. *Biomass and Bioenergy*, **35**(1), 298-307.

Chouchene, A., Jeguirim, M., Khiari, B., Zagrouba, F., Trouvé, G. 2010. Thermal degradation of olive solid waste: Influence of particle size and oxygen concentration. *Resources, Conservation and Recycling*, **54**(5), 271-277.

Demirbas, A. 2001. Biomass resource facilities and biomass conversion processing for fuels and chemicals. *Energy Conversion and Management*, **42**(11), 1357-1378.

Demirbas, A. 2004. Combustion characteristics of different biomass fuels. *Progress in Energy and Combustion Science*, **30**(2), 219-230.

Deng, Z., Xiao, R., Jin, B., Huang, H., Shen, L., Song, Q., Li, Q. 2008. Computational fluid dynamics modeling of coal gasification in a pressurized spout-fluid bed. *Energy & Fuels*, **22**(3), 1560-1569.

Didwania A, A.K., Robert, J. 2009. CFD Simulation of Scale-up of a DualL-Fluidized Bed Gasifier for Biomass.

Evans, R.J., Milne, T.A. 1987. Molecular characterization of the pyrolysis of biomass. *Energy & Fuels*, **1**(2), 123-137.

Fletcher, D., Haynes, B., Christo, F., Joseph, S. 2000. A CFD based combustion model of an entrained flow biomass gasifier. *Applied Mathematical Modelling*, **24**(3), 165-182.

Fu, P., Hu, S., Xiang, J., Li, P., Huang, D., Jiang, L., Zhang, A., Zhang, J. 2010. FTIR study of pyrolysis products evolving from typical agricultural residues. *Journal of analytical and applied pyrolysis*, **88**(2), 117-123.

Fu, P., Hu, S., Xiang, J., Sun, L., Yang, T., Zhang, A., Zhang, J. 2009. Mechanism Study of Rice Straw Pyrolysis by Fourier Transform Infrared Technique. *Chinese Journal of Chemical Engineering*, **17**(3), 522-529.

Gera, D., Gautam, M., Tsuji, Y., Kawaguchi, T., Tanaka, T. 1998. Computer simulation of bubbles in large-particle fluidized beds. *Powder technology*, **98**(1), 38-47.

Gerun, L., Paraschiv, M., Vijeu, R., Bellettre, J., Tazerout, M., Gøbel, B., Henriksen, U. 2008. Numerical investigation of the partial oxidation in a two-stage downdraft gasifier. *Fuel*, **87**(7), 1383-1393.

Ghetti, P., Ricca, L., Angelini, L. 1996. Thermal analysis of biomass and corresponding pyrolysis products. *Fuel*, **75**(5), 565-573.

Giuntoli, J., Arvelakis, S., Spliethoff, H., de Jong, W., Verkooijen, A.H.M. 2009. Quantitative and Kinetic Thermogravimetric Fourier Transform Infrared (TG-FTIR) Study of Pyrolysis of Agricultural Residues: Influence of Different Pretreatments. *Energy & Fuels*, **23**(11), 5695-5706.

Gómez-Barea, A., Leckner, B. 2010. Modeling of biomass gasification in fluidized bed. *Progress in Energy and Combustion Science*, **36**(4), 444-509.

Goyal, H., Seal, D., Saxena, R. 2008. Bio-fuels from thermochemical conversion of renewable resources: A review. *Renewable and Sustainable Energy Reviews*, **12**(2), 504-517.

Guide, F.U. 2011. Fluent.

Hall, D.O. 1997. Biomass energy in industrialised countries - A view of the future. *Forest Ecology and Management*, **91**(1), 17-45.

Hanaoka, T., Inoue, S., Uno, S., Ogi, T., Minowa, T. 2005. Effect of woody biomass components on air-steam gasification. *Biomass and Bioenergy*, **28**(1), 69-76.

Haykiri-Acma, H., Yaman, S., Kucukbayrak, S. 2006. Effect of heating rate on the pyrolysis yields of rapeseed. *Renewable Energy*, **31**(6), 803-810.

Hill, J., Nelson, E., Tilman, D., Polasky, S., Tiffany, D. 2006. Environmental, economic, and energetic costs and benefits of biodiesel and ethanol biofuels. *Proceedings of the National Academy of Sciences*, **103**(30), 11206.

Ibsen, C.H., Helland, E., Hjertager, B.H., Solberg, T., Tadrist, L., Occelli, R. 2004. Comparison of multifluid and discrete particle modelling in numerical predictions of gas particle flow in circulating fluidised beds. *Powder technology*, **149**(1), 29-41.

Jefferson, P.G., McCaughey, W.P., May, K., Woosaree, J., McFarlane, L. 2004. Potential utilization of native prairie grasses from western Canada as ethanol feedstock. *Canadian journal of plant science*, **84**(4), 1067-1075.

Jeguirim, M., Trouvé, G. 2009. Pyrolysis characteristics and kinetics of Arundo donax using thermogravimetric analysis. *Bioresource Technology*, **100**(17), 4026-4031.

Johnson, D., Adam, P., Ashley, P., Chum, H., Deutch, S., Fennel, J., Wiselogel, A. 1994. Study of compositional changes in biomass feedstocks upon storage (results). *Rapport-Sveriges Lantbruksuniversitet, Institutionen foer Virkeslaera*.

Keshwani, D.R., Cheng, J.J. 2009. Switchgrass for bioethanol and other value-added applications: A review. *Bioresource Technology*, **100**(4), 1515-1523.

Kim, Y., Mosier, N.S., Hendrickson, R., Ezeji, T., Blaschek, H., Dien, B., Cotta, M., Dale, B., Ladisch, M.R. 2008. Composition of corn dry-grind ethanol by-products: DDGS, wet cake, and thin stillage. *Bioresource Technology*, **99**(12), 5165-5176.

Klass, D.L. 1995. Biomass energy in North American policies. *Energy Policy*, **23**(12), 1035-1048.

Kuipers, J., Prins, W., Van Swaaij, W. 1992. Numerical calculation of wall to bed heat transfer coefficients in gas fluidized beds. *AIChE journal*, **38**(7), 1079-1091.

Kumar, A., Eskridge, K., Jones, D.D., Hanna, M.A. 2009a. Steam-air fluidized bed gasification of distillers grains: Effects of steam to biomass ratio, equivalence ratio and gasification temperature. *Bioresour Technol*, **100**(6), 2062-2068.

Kumar, A., Noureddini, H., Demirel, Y., Jones, D., Hanna, M. 2009b. Simulation of corn stover and distillers grains gasification with Aspen Plus. *Transactions of the ASAE*, **52**(6), 1989-1995.

Kumar, A., Wang, L., Dzenis, Y.A., Jones, D.D., Hanna, M.A. 2008a. Thermogravimetric characterization of corn stover as gasification and pyrolysis feedstock. *Biomass and Bioenergy*, **32**(5), 460-467.

Kumar, A., Wang, L.J., Dzenis, Y.A., Jones, D.D., Hanna, M.A. 2008b. Thermogravimetric characterization of corn stover as gasification and pyrolysis feedstock. *Biomass & Bioenergy*, **32**(5), 460-467.

Kumar, V. 2009. Pyrolysis and gasification of lignin and effect of alkali addition, Vol. Ph.D., Georgia Institute of Technology. United States -- Georgia, pp. 179.

Kutler, P. 1989. Computational fluid dynamic-current capabilities and directions for the future. ACM. pp. 113-122.

Lavoie, J., Chaouki, J., Drouin, G. 2006. Biomass Gasification in a Bubbling Fluidized bed: Numerical Modeling and Experiments.

Lee, D.K., Owens, V. 2005. Biomass production potential of native warm-season grass monocultures and mixtures.

Lee, S.-B., Fasina, O. 2009. TG-FTIR analysis of switchgrass pyrolysis. *Journal of analytical and applied pyrolysis*, **86**(1), 39-43.

Lettner, F., Timmerer, H., Haselbacher, P. 2007. Biomass gasification–State of the art description. *Graz Univ. Tech.-Institute of thermal engineering*.

Lewellen, P., Peters, W., Howard, J. 1977. Cellulose pyrolysis kinetics and char formation mechanism. Elsevier. pp. 1471-1480.

Li, S., Lyons-Hart, J., Banyasz, J., Shafer, K. 2001. Real-time evolved gas analysis by FTIR method: an experimental study of cellulose pyrolysis. *Fuel*, **80**(12), 1809-1817.

Liu, L., Ye, X.P., Womac, A.R., Sokhansanj, S. 2010. Variability of biomass chemical composition and rapid analysis using FT-NIR techniques. *Carbohydrate Polymers*, **81**(4), 820-829.

Liu, Q., Wang, S., Zheng, Y., Luo, Z., Cen, K. 2008. Mechanism study of wood lignin pyrolysis by using TG-FTIR analysis. *Journal of Analytical and Applied Pyrolysis*, **82**(1), 170-177.

Lv, P., Xiong, Z., Chang, J., Wu, C., Chen, Y., Zhu, J. 2004. An experimental study on biomass air-steam gasification in a fluidized bed. *Bioresource Technology*, **95**(1), 95-101.

Mani, T., Murugan, P., Abedi, J., Mahinpey, N. 2010a. Pyrolysis of wheat straw in a thermogravimetric analyzer: Effect of particle size and heating rate on devolatilization and estimation of global kinetics. *Chemical Engineering Research and Design*, **In Press, Corrected Proof**.

Mani, T., Murugan, P., Abedi, J., Mahinpey, N. 2010b. Pyrolysis of wheat straw in a thermogravimetric analyzer: Effect of particle size and heating rate on devolatilization and estimation of global kinetics. *Chemical Engineering Research and Design*, **88**(8), 952-958.

Mansaray, K.G., Ghaly, A.E. 1999. Determination of Reaction Kinetics of Rice Husks in Air Using Thermogravimetric Analysis. *Energy Sources, Part A: Recovery, Utilization, and Environmental Effects*, **21**(10), 899 - 911.

Marklund, M., Tegman, R., Gebart, R. 2007. CFD modelling of black liquor gasification: Identification of important model parameters. *Fuel*, **86**(12-13), 1918-1926.

Massé, D., Gilbert, Y., Savoie, P., Bélanger, G., Parent, G., Babineau, D. 2010. Methane yield from switchgrass harvested at different stages of development in Eastern Canada. *Bioresource Technology*, **101**(24), 9536-9541.

Meier, D., Faix, O. 1999. State of the art of applied fast pyrolysis of lignocellulosic materials--a review. *Bioresource Technology*, **68**(1), 71-77.

Mészáros, E., Várhegyi, G., Jakab, E., Marosvölgyi, B. 2004. Thermogravimetric and Reaction Kinetic Analysis of Biomass Samples from an Energy Plantation. *Energy & Fuels*, **18**(2), 497-507.

Miranda, R., Sosa_Blanco, C., Bustos-Martínez, D., Vasile, C. 2007. Pyrolysis of textile wastes: I. Kinetics and yields. *Journal of Analytical and Applied Pyrolysis*, **80**(2), 489-495.

Mohan, D., Pittman, C.U., Jr., Steele, P.H. 2006. Pyrolysis of wood/biomass for bio-oil: A critical review. *Energy & Fuels*, **20**(3), 848-889.

Mulkey, V., Lee, V. 2006. Management of switchgrass-dominated conservation reserve program lands for biomass production in South Dakota. *Crop Science*, **46**(2), 712.

Munir, S., Daood, S.S., Nimmo, W., Cunliffe, A.M., Gibbs, B.M. 2009. Thermal analysis and devolatilization kinetics of cotton stalk, sugar cane bagasse and shea meal under nitrogen and air atmospheres. *Bioresource Technology*, **100**(3), 1413-1418.

Murugan, P., Mahinpey, N., Johnson, K.E., Wilson, M. 2008. Kinetics of the pyrolysis of lignin using thermogravimetric and differential scanning calorimetry methods. *Energy & Fuels*, **22**(4), 2720-2724.

Nada, A., Hassan, M.L. 2000. Thermal behavior of cellulose and some cellulose derivatives. *Polymer degradation and stability*, **67**(1), 111-115.

Oevermann, M., Gerber, S., Behrendt, F. 2009. Euler-Lagrange/DEM simulation of wood gasification in a bubbling fluidized bed reactor. *Particuology*, **7**(4), 307-316.

Orfão, J.J.M., Antunes, F.J.A., Figueiredo, J.L. 1999. Pyrolysis kinetics of lignocellulosic materials—three independent reactions model. *Fuel*, **78**(3), 349-358.

Ounas, A., Aboulkas, A., El harfi, K., Bacaoui, A., Yaacoubi, A. 2011. Pyrolysis of olive residue and sugar cane bagasse: Non-isothermal thermogravimetric kinetic analysis. *Bioresource Technology*, **102**(24), 11234-11238.

Pasquali, C., Herrera, H. 1997. Pyrolysis of lignin and IR analysis of residues. *Thermochimica acta*, **293**(1-2), 39-46.

Patil, D., Smit, J., van Sint Annaland, M., Kuipers, J. 2006. Wall to bed heat transfer in gas–solid bubbling fluidized beds. *AIChE journal*, **52**(1), 58-74.

Pérez, J., Munoz-Dorado, J., De la Rubia, T., Martinez, J. 2002. Biodegradation and biological treatments of cellulose, hemicellulose and lignin: an overview. *International Microbiology*, **5**(2), 53-63.

Ramiah, M. 1970. Thermogravimetric and differential thermal analysis of cellulose, hemicellulose, and lignin. *Journal of Applied Polymer Science*, **14**(5), 1323-1337.

Raveendran, K., Ganesh, A., Khilar, K.C. 1996. Pyrolysis characteristics of biomass and biomass components. *Fuel*, **75**(8), 987-998.

Rogel, A., Aguillón, J. 2006. The 2D Eulerian approach of entrained flow and temperature in a biomass stratified downdraft gasifier. *American Journal of Applied Sciences*, **3**(10), 2068-2075.

Ryu, C., Yang, Y.B., Khor, A., Yates, N.E., Sharifi, V.N., Swithenbank, J. 2006. Effect of fuel properties on biomass combustion: Part I. Experiments—fuel type, equivalence ratio and particle size. *Fuel*, **85**(7-8), 1039-1046.

Schmidt, A., Renz, U. 2000. Numerical prediction of heat transfer in fluidized beds by a kinetic theory of granular flows. *International Journal of Thermal Sciences*, **39**(9-11), 871-885.

Shafizadeh, F., McGinnis, G.D., Philpot, C.W. 1972. Thermal degradation of xylan and related model compounds. *Carbohydrate Research*, **25**(1), 23-33.

Shen, D.K., Gu, S. 2009. The mechanism for thermal decomposition of cellulose and its main products. *Bioresource Technology*, **100**(24), 6496-6504.

Shen, D.K., Gu, S., Bridgwater, A.V. 2010. Study on the pyrolytic behaviour of xylan-based hemicellulose using TG-FTIR and Py-GC-FTIR. *Journal of Analytical and Applied Pyrolysis*, **87**(2), 199-206.

Singh, S., Wu, C., Williams, P.T. 2012. Pyrolysis of waste materials using TGA-MS and TGA-FTIR as complementary characterisation techniques. *Journal of analytical and applied pyrolysis*, **94**(0), 99-107.

Skreiberg, A., Skreiberg, Ø., Sandquist, J., Sørum, L. 2011. TGA and macro-TGA characterisation of biomass fuels and fuel mixtures. *Fuel*, **90**(6), 2182-2197.

Sundaresan, S. 2000. Modeling the hydrodynamics of multiphase flow reactors: current status and challenges. *AIChE journal*, **46**(6), 1102-1105.

Tilman, D., Hill, J., Lehman, C. 2006. Carbon-negative biofuels from low-input high-diversity grassland biomass. *Science*, **314**(5805), 1598.

Vamvuka, D., Kakaras, E., Kastanaki, E., Grammelis, P. 2003a. Pyrolysis characteristics and kinetics of biomass residuals mixtures with lignite[small star, filled]. *Fuel*, **82**(15-17), 1949-1960.

Vamvuka, D., Kakaras, E., Kastanaki, E., Grammelis, P. 2003b. Pyrolysis characteristics and kinetics of biomass residuals mixtures with lignite☆. *Fuel*, **82**(15–17), 1949-1960.

Wang, C., Wu, Y., Liu, Q., Yang, H., Wang, F. 2011. Analysis of the behaviour of pollutant gas emissions during wheat straw/coal cofiring by TG–FTIR. *Fuel Processing Technology*, **92**(5), 1037-1041.

Wang, L., Kumar, A., Hanna, M., Weller, C.L., Jones, D. 2009. Thermal Degradation Kinetics of Distillers Grains and Solubles in Nitrogen and Air. *Energy Sources, Part A*, **31**(10), 797-806.

Westbrook, C.K., Mizobuchi, Y., Poinsot, T.J., Smith, P.J., Warnatz, J. 2005. Computational combustion. *Proceedings of the combustion Institute*, **30**(1), 125-157.

Wiselogel, A.E., Agblevor, F.A., Johnson, D.K., Deutch, S., Fennell, J.A., Sanderson, M.A. 1996. Compositional changes during storage of large round switchgrass bales. *Bioresource Technology*, **56**(1), 103-109.

Xie, W., Pan, W.P. 2001. Thermal characterization of materials using evolved gas analysis. *Journal of thermal analysis and calorimetry*, **65**(3), 669-685.

Yan, R., Yang, H., Chin, T., Liang, D.T., Chen, H., Zheng, C. 2005. Influence of temperature on the distribution of gaseous products from pyrolyzing palm oil wastes. *Combustion and Flame*, **142**(1-2), 24-32.

Yang, H., Yan, R., Chen, H., Lee, D.H., Zheng, C. 2007. Characteristics of hemicellulose, cellulose and lignin pyrolysis. *Fuel*, **86**(12–13), 1781-1788.

Yang, H., Yan, R., Chin, T., Liang, D.T., Chen, H., Zheng, C. 2004. Thermogravimetric Analysis−Fourier Transform Infrared Analysis of Palm Oil Waste Pyrolysis. *Energy & Fuels*, **18**(6), 1814-1821.

Yu, L., Lu, J., Zhang, X., Zhang, S. 2007. Numerical simulation of the bubbling fluidized bed coal gasification by the kinetic theory of granular flow (KTGF). *Fuel*, **86**(5-6), 722-734.

Zhang, X., Xu, M., Sun, R., Sun, L. 2006. Study on Biomass Pyrolysis Kinetics. *Journal of Engineering for Gas Turbines and Power*, **128**(3), 493-496.

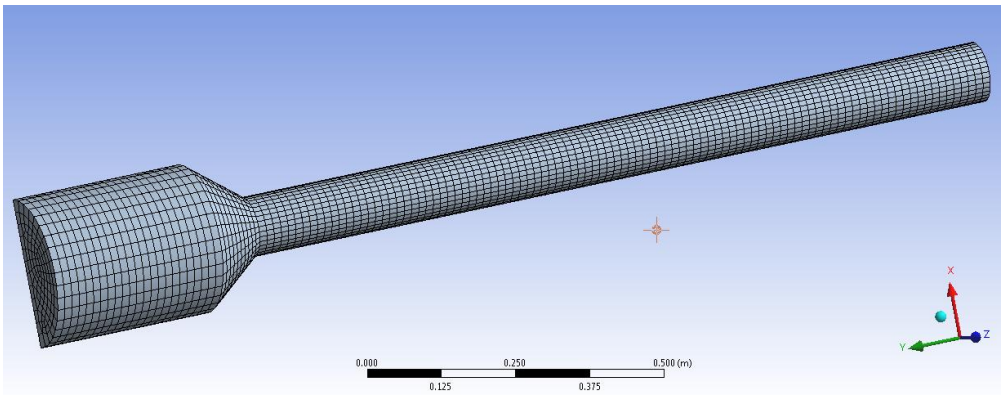

Figure 1. Computational set up of fluidized bed reactor

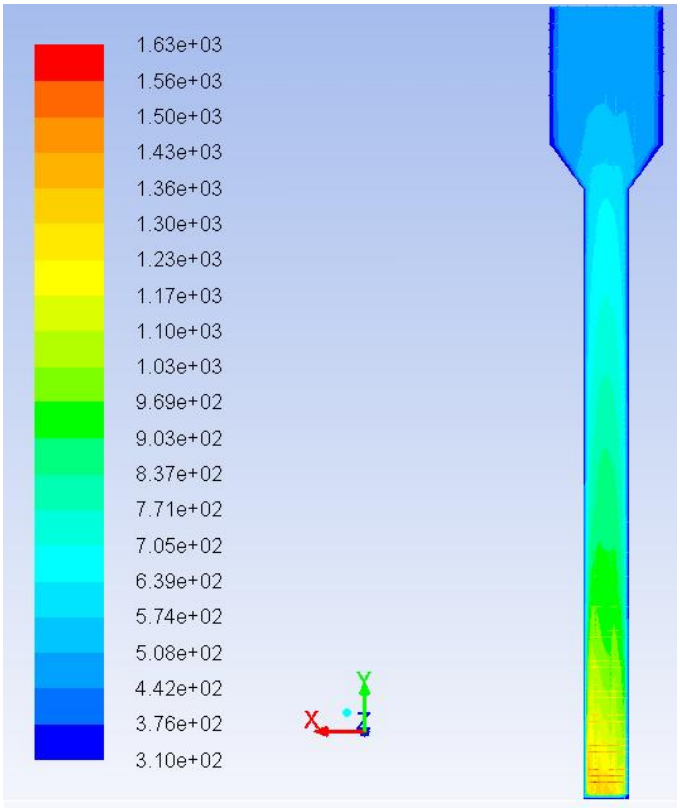

Figure 2. Contour representing the temperature distribution inside the gasifier

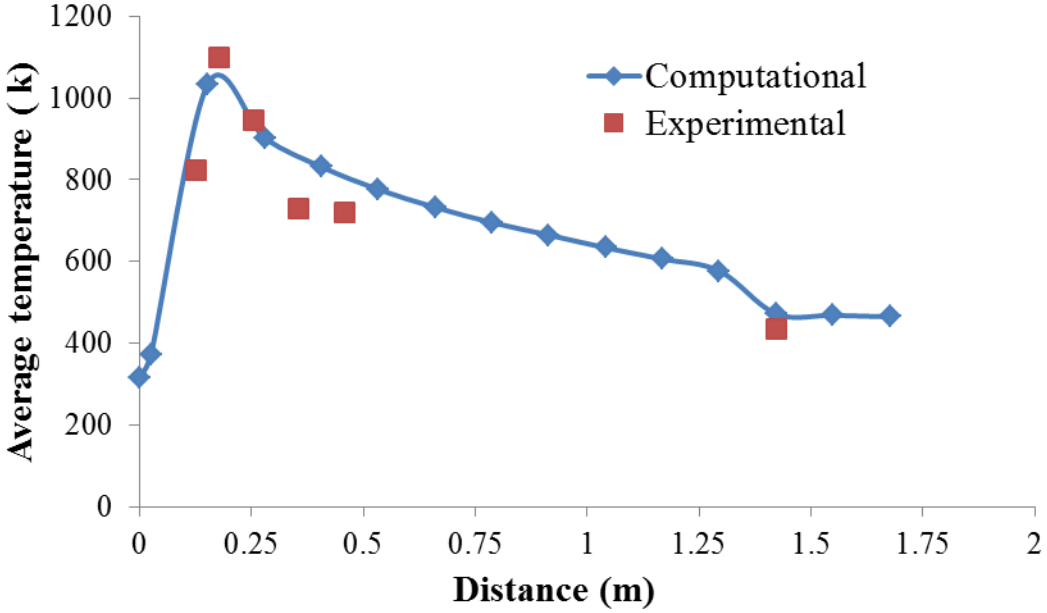

Figure 3. Average axial temperature distribution profile

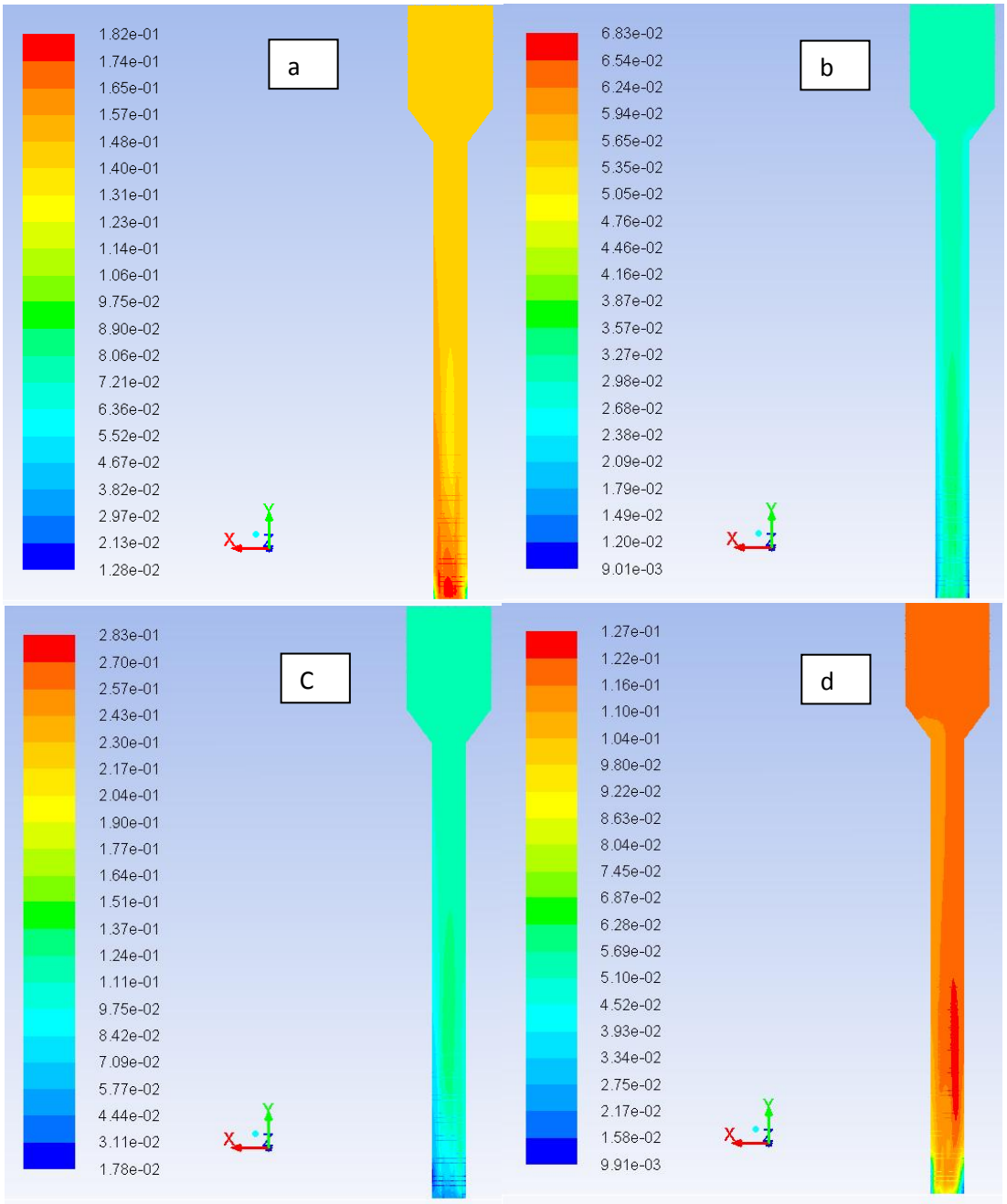

Figure 4. Time average mole fraction contours of (a) CO_2 (b) CH_4 (C) CO (d) H_2

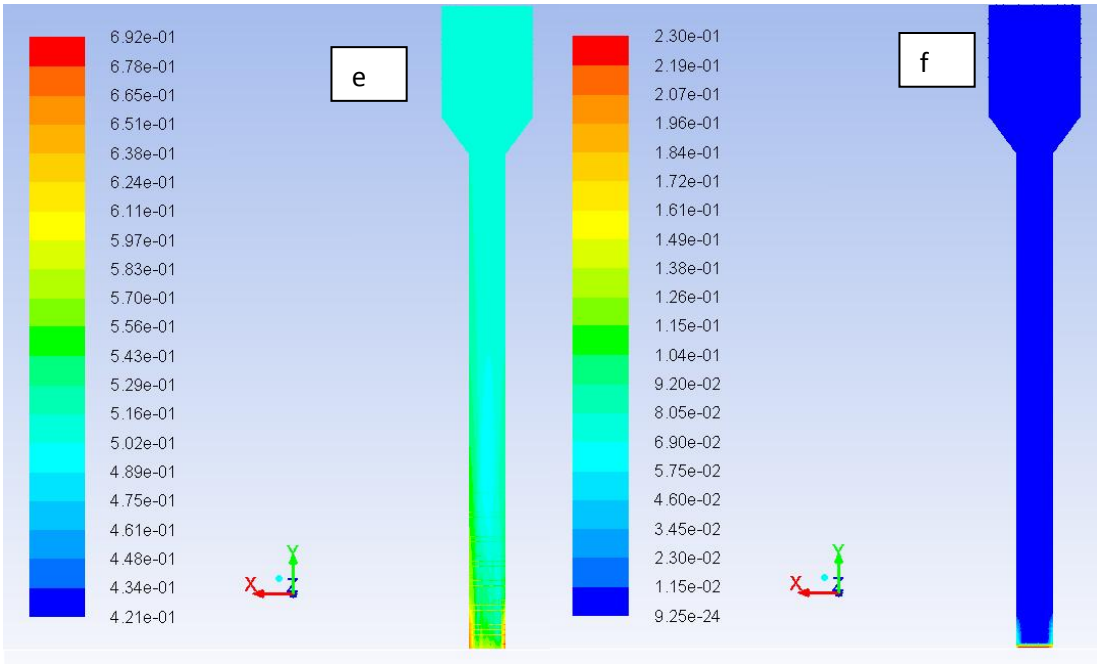

Figure 5. Time averaged mole fraction contours of (e) N_2 (f) O_2

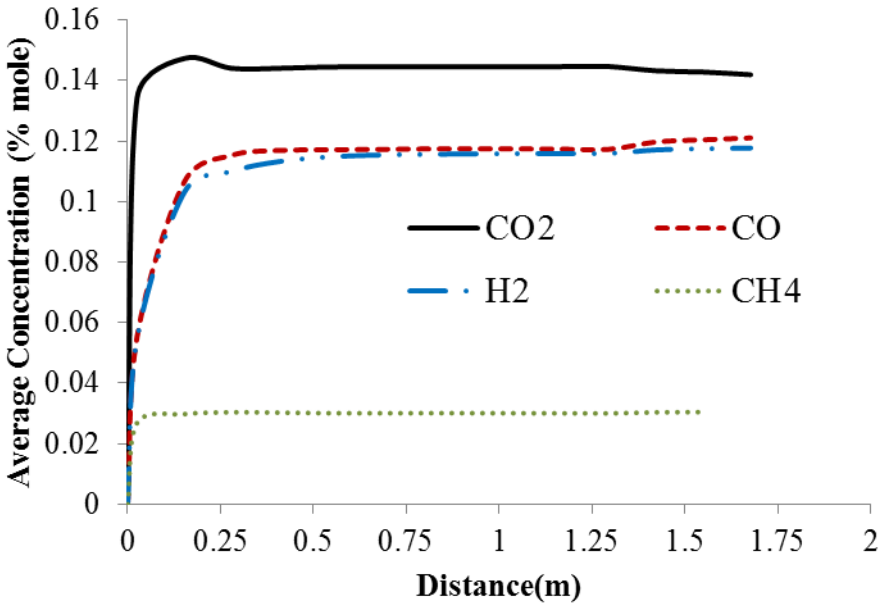

Figure 6. Average axial concentration profiles of CO, CO_2, CH_4, and H_2

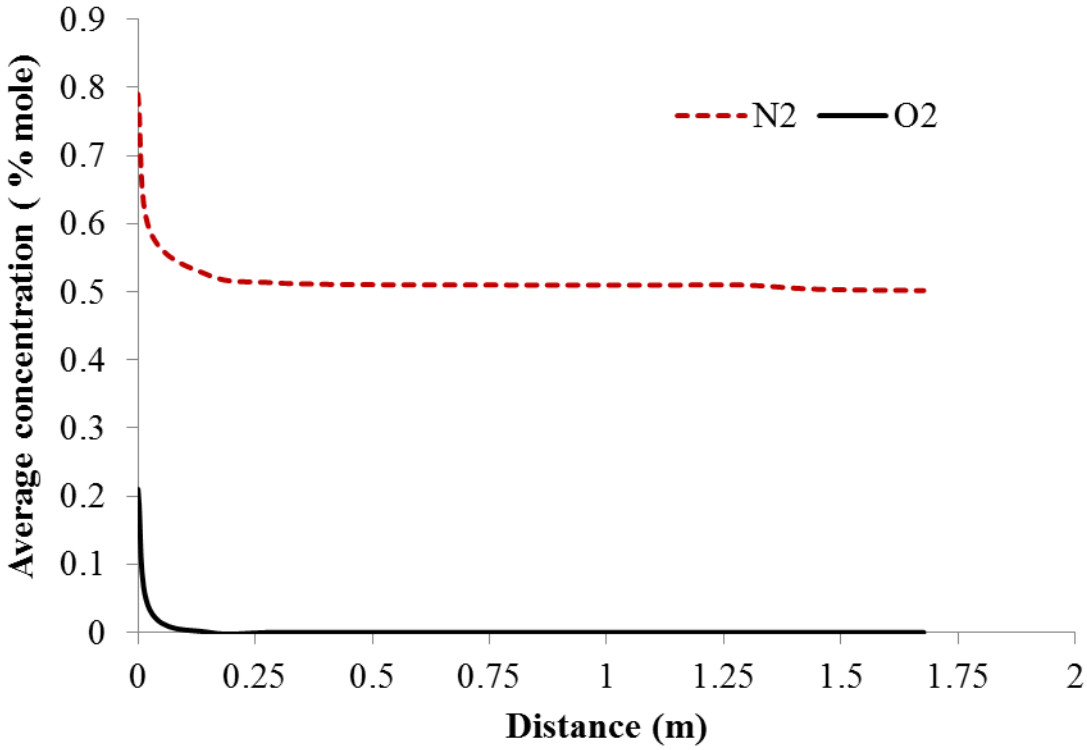

Figure 7. Average axial concentration profiles of N_2 and O_2

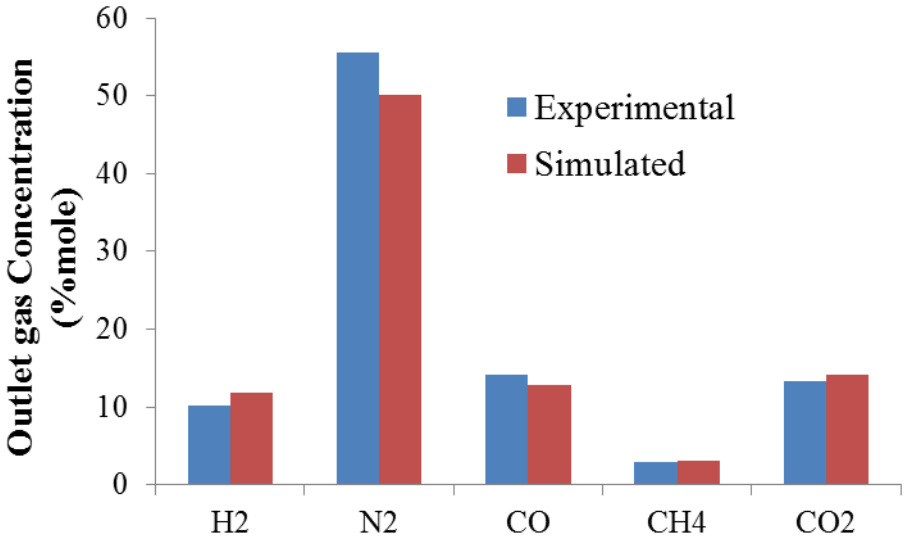

(a)

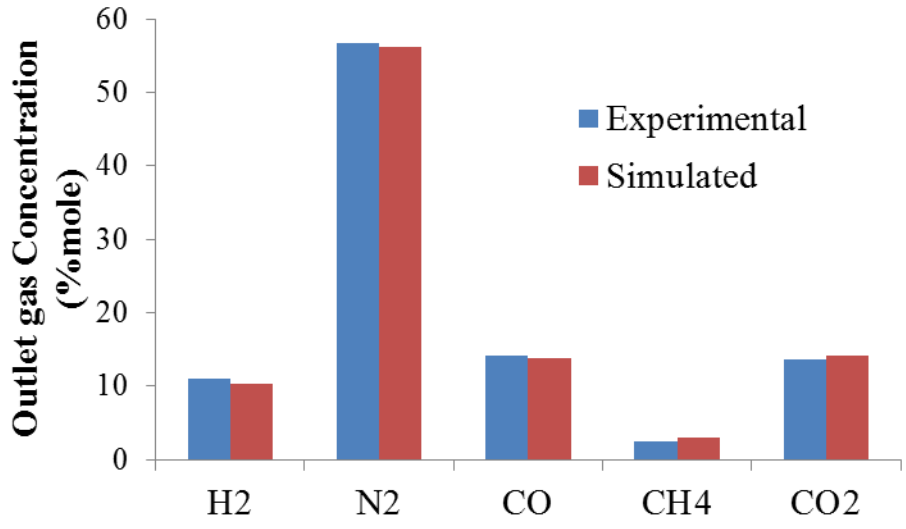

(b)

Figure 8. Gas concentrations at the outlet of the gasifier for (a) ER=0.32 (b) ER=0.29

Table 1. Reaction kinetic parameters used in CFD modeling

Reactions	Heat of reaction (KJ/mol)	A (1/s)	E(kJ/mol)
Devolatilization reaction	-118.12	3.88E+10	103.7
Homogeneous reactions			
$CO+H_2O \leftrightarrow H_2+CO_2$	-41.15	0.0265	65.8
$CO+0.5O_2 \rightarrow CO_2$	-338.26	8.83E+11	100
$H_2+0.5O2 \rightarrow H_2O$	-241.84	3.09E+11	100
$CH_4+1.5O_2 \rightarrow CO+H_2O$	-277.48	1.58E+08	202
Heterogeneous reactions			
$C<S>+O_2 \rightarrow CO_2$	-393.53	9.35E+04	82.8
$C<S>+CO_2 \rightarrow 2CO$	172.45	3.62E+01	77.39
$C<S>+2H_2 \rightarrow CH_4$	-74.90	4.20E-03	19.21
$C<S>+H_2O \rightarrow CO+H_2$	131.30	1.52E+04	121.62

Table 2. Proximate and Ultimate analyses of switchgrass

	Proximate Analysis		Ultimate Analysis
Moisture (%, w.b.)	9.7	Carbon	46.62%
Volatile matter (% d.b.)	80.36	Hydrogen	5.74%
Ash (% d.b.)	4.62	Oxygen	42.27%
Fixed carbon (% d.b.)	15.02	Nitrogen	<0.3%
HHV of dry biomass (MJ kg^{-1}, d.b.)	18.83	Sulfur	

CHAPTER V

Recommendations

The present study provided the fundamental information required to understand the biomass devolatilization process. Based on the results from the present work, the following aspects are recommended for future research in the biomass thermochemical conversion process.

The devolatilization kinetics of switchgrass was used to develop a Computational Fluid Dynamics model which is capable of predicting the gas and temperature profiles inside a fluidized bed reactor. TGA-FTIR studies also provided devolatilization kinetic data for red cedar, wheat straw, cellulose, hemicellulose and lignin. The model can utilize this kinetic data and simulate gasification to predict gas profiles and temperature distribution inside the gasifier. Moreover, the effect of operating parameters such as bed height, bed material and temperature also can be examined using the CFD model.

APPPENDICES

APPENDIX A.

Table.1 Fluent models and input summary

SOLVER CONTROLS	
solver	3D segregated
velocity formulation	absolute
Gradient option	cell-based
Formulation	implicit
Time	unsteady
SPECIES MODEL	
model	species transport
reactions	volumetric, surface
turb-chemical interaction	Eddy-dissipation and Arrhenius rate
MULTIPHASE MODEL	
model	eulerian-lagrangian
TURBULENT MODEL	
k-epsilon model	realizable
Near wall treatment	standard

Table 2. Properties of CO, CO_2, CH_4 and H_2

	CO	CO_2	CH_4	H_2
Material type	fluid	fluid	fluid	fluid
Molecular weight	28	44	16	2
Standard state enthalpy	-1.11E+08	-3.94E+08	-7.49E+07	-1.88E+03
Standard state entropy	197535.7	213720.2	186043.29	130581.7
Reference temperature	298	298	298	298
Cp	Piecewise-polynomial	Piecewise-polynomial	Piecewise-polynomial	Piecewise-polynomial

VITA

Vamsee Pasangulapati

Candidate for the Degree of

Master of Science

Thesis: DEVOLATILIZATION CHARACTERISTICS OF CELLULOSE, HEMICELLULOSE AND LIGNIN AND THE SELECTED BIOMASS DURING THERMOCHEMICAL GASIFICATION: EXPERIMENT AND MODELING STUDIES

Major Field: Biosystems and Agricultural Engineering

Biographical:

Education:

Completed the requirements for the Master of Science in Biosystems and Agricultural Engineering at Oklahoma State University, Stillwater, Oklahoma in December, 2012.

Completed the requirements for the Bachelors of Technology in Mechanical Engineering at CMR Engineering and Technology affiliated to Jawaharlal Nehru Technological University, Hyderabad, India in May, 2007.

Experience:
Graduate Research Assistant under Dr. Ajay Kumar from January 2010 to January 2012

Professional Memberships: ASABE

Name: Vamsee Pasangulapati Date of Degree: May, 2012

Institution: Oklahoma State University Location: Stillwater, Oklahoma

Title of Study: DEVOLATILIZATION CHARACTERISTICS OF CELLULOSE, HEMICELLULOSE AND LIGNIN AND THE SELECTED BIOMASS DURING THERMOCHEMICAL GASIFICATION: EXPERIMENT AND MODELING STUDIES

Pages in Study: 108 Candidate for the Degree of Master of Science

Major Field: Biosystems and Agricultural Engineering

Pyrolysis and gasification are two promising thermochemical conversion technologies for conversion of biomass into fuels, chemicals and power. Devolatilization is the first major process that occurs in biomass gasification and pyrolysis. Thus it is essential to study the fundamentals of biomass devolatilization, which helps in better understanding, modeling and optimization of biomass thermochemical conversion processes.

The devolatilization characteristics of biomass major components cellulose, hemicellulose and lignin were investigated using thermogravimetric analysis. The weight loss kinetics were derived using global decomposition approach. Spectral analysis was conducted and major gases such as CO, CO_2 and CH_4 were identified along with hydrocarbons, alcohols, ketones and acids.

The devolatilization characteristics of switchgrass, wheat straw, eastern red cedar and DDGS were investigated using thermogravimetric analysis. The focus of this objective was to investigate how the biomass components contributed to yields and properties of products during devolatilization. Results show that the effect of biomass composition on thermal degradation profiles and weight loss kinetics was not significant. However, with change in biomass composition, significant effects were observed on CO, CO_2 and CH_4 evolution profiles. Carbon based conversion efficiency was higher for switchgrass (94.2%) and wheat straw (95.0%) and lower for red cedar (77.0%) and DDGS (76.8%).

A CFD model for switchgrass gasification in a fluidized bed reactor was developed using devolatilization kinetics obtained from thermogravimetric analysis. The simulation results provided detailed information on temperature and gas concentration profiles inside the reactor. The non-uniform distribution of temperature in the reactor showed the different reaction zones for devolatilization, combustion and gasification. The model validation was performed by comparing the predicted outlet concentrations of the gases with experimental data. The sensitivity of the model was also analyzed by simulating at two equivalence ratios of 0.32 and 0.29.

ADVISER'S APPROVAL: Dr. Ajay Kumar